IOP Publishing Plasma Physics and Controlled Fusion
Plasma Phys. Control. Fusion 59 (2017) 125005 (22pp) https://doi.org/10.1088/1361-6587/aa8c49

Tests of a two-color interferometer and polarimeter for ITER density measurements

M A Van Zeeland[1], T N Carlstrom[1], D K Finkenthal[2], R L Boivin[1], A Colio[2], D Du[1], A Gattuso[1], F Glass[1], C M Muscatello[1], R O'Neill[1], M Smiley[1], J Vasquez[1], M Watkins[1], D L Brower[3], J Chen[3], W X Ding[3], D Johnson[4], P Mauzey[1], M Perry[5], C Watts[6] and R Wood[4]

[1] General Atomics, PO Box 85608 San Diego, CA 92186-5608, United States of America
[2] Palomar Scientific Instruments, San Marcos, CA 92069, United States of America
[3] Department of Physics and Astronomy, University of California Los Angeles, Los Angeles, CA 90095, United States of America
[4] Princeton Plasma Physics Laboratory, PO Box 451, Princeton, NJ 08543-0451, United States of America
[5] Cal State University, San Marcos, San Marcos, CA 92096, United States of America
[6] ITER Organization, Route de Vinon-sur-Verdon, CS 90 046, F-13067 St. Paul Lez Durance Cedex, France

E-mail: vanzeeland@fusion.gat.com

Received 27 June 2017, revised 30 August 2017
Accepted for publication 13 September 2017
Published 25 October 2017

Abstract

A full-scale 120 m path length ITER toroidal interferometer and polarimeter (TIP) prototype, including an active feedback alignment system, has been constructed and undergone initial testing at General Atomics. In the TIP prototype, two-color interferometry is carried out at 10.59 μm and 5.22 μm using a CO_2 and quantum cascade laser (QCL) respectively while a separate polarimetry measurement of the plasma induced Faraday effect is made at 10.59 μm. The polarimeter system uses co-linear right and left-hand circularly polarized beams upshifted by 40 and 44 MHz acousto-optic cells respectively, to generate the necessary beat signal for heterodyne phase detection, while interferometry measurements are carried out at both 40 MHz and 44 MHz for the CO_2 laser and 40 MHz for the QCL. The high-resolution phase information is obtained using an all-digital FPGA based phase demodulation scheme and precision clock source. The TIP prototype is equipped with a piezo tip/tilt stage active feedback alignment system responsible for minimizing noise in the measurement and keeping the TIP diagnostic aligned indefinitely on its 120 m beam path including as the ITER vessel is brought from ambient to operating temperatures. The prototype beam path incorporates translation stages to simulate ITER motion through a bake cycle as well as other sources of motion or misalignment. Even in the presence of significant motion, the TIP prototype is able to meet ITER's density measurement requirements over 1000 s shot durations with demonstrated phase resolution of 0.06° and 1.5° for the polarimeter and vibration compensated interferometer respectively. TIP vibration compensated interferometer measurements of a plasma have also been made in a pulsed radio frequency device and show a line-integrated density resolution of $\delta nL = 3.5 \times 10^{17}$ m^{-2}.

Supplementary material for this article is available online

Keywords: interferometry, plasma diagnostics, electron density measurement, ITER, Tokamak

(Some figures may appear in colour only in the online journal)

1. Introduction

The primary system planned for real-time density control in ITER is the five channel combined toroidal interferometer and polarimeter (TIP). TIP will also contribute to density profile reconstruction and play a secondary role as a diagnostic of core density fluctuations including those from broadband turbulence, MHD, and other coherent modes such as Alfvén eigenmodes. [1] Initial design studies of the TIP based on CO_2 and CO lasers were carried out in 1998 [2, 3] and, in 2013, following a successful conceptual design review, a more detailed design was published [4]. This paper describes the design, construction and initial testing of a full-scale ITER TIP prototype including feedback alignment.

The TIP prototype discussed here is largely based on the 2013 design and makes a two-color interferometry [5–9] measurement at 10.59 and 5.22 μm using a CO_2 and quantum cascade laser (QCL) respectively, while a separate polarimetry measurement of the plasma induced Faraday effect by launching right-hand and left-hand polarized waves, utilizing the Dodel and Kunz technique [10–14], is made at 10.59 μm. In this configuration, each beam of the two-color vibration compensated interferometer with wavelength λ_i, experiences a phase shift ϕ_i due to vibration (V) and plasma with electron density n_e and temperature T_e given by

$$\phi_i = r_e \lambda_i \int n_e \left(1 - \tfrac{3}{2}\tau + \tfrac{15}{8}\tau^2\right) \mathrm{d}L + \frac{2\pi V}{\lambda_i}, \qquad (1)$$

where $\tau = \frac{T_e}{m_e c^2}$, $r_e = 2.82 \times 10^{-15}$ m (the classical electron radius) and m_e the electron mass [15, 16]. Note, the interferometric phase shift and Faraday rotation angles shown above and in equation (4) below respectively, include recent approximations for finite electron temperature corrections derived to accurately include the impact of electron thermal motion with all relativistic effects taken into account [16]. For low temperatures, the line-integrated density measured by the two-color interferometer becomes

$$\int n_e \mathrm{d}L = \frac{\lambda_{CO_2}}{r_e(\lambda_{CO_2}^2 - \lambda_{QCL}^2)} \left[\phi_{CO_2} - \frac{\lambda_{QCL}}{\lambda_{CO_2}} \phi_{QCL}\right]. \qquad (2)$$

The quantity that will be referred to in this document as the 'vibration compensated phase' is given by

$$\phi_{int} = \left[\phi_{CO_2} - \frac{\lambda_{QCL}}{\lambda_{CO_2}} \phi_{QCL}\right]. \qquad (3)$$

The Faraday rotation (α) experienced by the TIP beam is given by

$$\alpha = C_p \lambda_{CO_2}^2 \int n_e (1 - 2\tau + 3\tau^2) \vec{B} \cdot \mathrm{d}\vec{L}, \qquad (4)$$

where B is the local magnetic field, and $C_p = 2.62 \times 10^{-13}$ rad T^{-1} [15, 16]. At low electron temperatures, the polarimeter experiences a phase shift (ϕ_{pol}), which is twice the Faraday rotation angle and is given by:

$$\phi_{pol} = 2 C_p \lambda_{CO_2}^2 \int n_e \vec{B} \cdot \mathrm{d}\vec{L}. \qquad (5)$$

In [4], simulations of the expected TIP signals during a 15 MA baseline scenario discharge found that the maximum measured interferometer phase shift corresponds to roughly ten full CO_2 fringes while the measured Faraday rotation angle is always less than a full fringe, eliminating any possible phase ambiguity. In fact, the polarimeter measured phase shift is always less than 2π even for line-averaged densities up to the Greenwald density of approximately 1.2×10^{20} m^{-3}. Thus, in the event of a fringe skip in the interferometer system, one would be able to renormalize using the polarimeter measurement. The original specified accuracy of the line-averaged density measurement by TIP was 1% as given in table 2 of [1], which has been relaxed somewhat to 10% during current ramp-up and 2% during flattop [17] with a bandwidth of 1 kHz. As discussed in [4], a CO_2 laser based TIP system is able to fulfill (or exceed) these requirements with a vibration compensated phase resolution of $\delta\phi_{int} < 10^\circ$ and polarimeter phase resolution of $\delta\phi_{pol} < 0.1^\circ$, which are taken as the target values for the work presented here. The precision with which ϕ_{int} and ϕ_{pol} can be measured, however, depends critically on several parameters including the relative beam alignment, alignment stability, laser wavelength stability, position on detector, detector noise, etc.

All elements of the laser based TIP system are susceptible to misalignment errors of its probe beams and are only partially tolerant to beam path motion. For example, the two-color interferometer is able to effectively cancel vibration parallel to the beam path, as is the polarimeter. Both, however, are sensitive to any motion perpendicular to the beam and, in the case of the polarimeter, this can be the largest source of noise for even millimeter level perpendicular displacements on the detector [12, 13]. Between initial TIP alignment, performed when the vacuum vessel is at room temperature, and operation at 70 °C, port plug displacements due to the thermal expansion are anticipated to be approximately one centimeter and several centimeters from ambient alignment temperature to that at bake. Shot to shot variability of the port plug position is expected to be approximately 1−2 mm. During a pulse, beam displacements on the order of 1 mm are expected due to various sources of vibration and potentially density gradient induced refraction. It is also expected that diagnostic hall temperature variations will cause mirror shifting and steering throughout the day as well potentially drifts over longer timescales. While the majority of these expected displacements are not large, they can have a significant impact on TIP performance and signal levels, yet cannot realistically be compensated for by human based adjustment thus some form of automated or feedback alignment will be essential. In addition to the actual interferometer and polarimeter, this paper also describes a preliminary piezo tip/tilt stage based prototype feedback alignment system that helps the TIP system meet ITER's measurement requirements in the presence of significant motion, maintain alignment with minimal intervention, minimize beam clipping and diffraction from aperture edges and the ability to handle beam interruption.

This paper is organized as the TIP R&D program was, in three stages, with bench testing of a lab prototype followed by

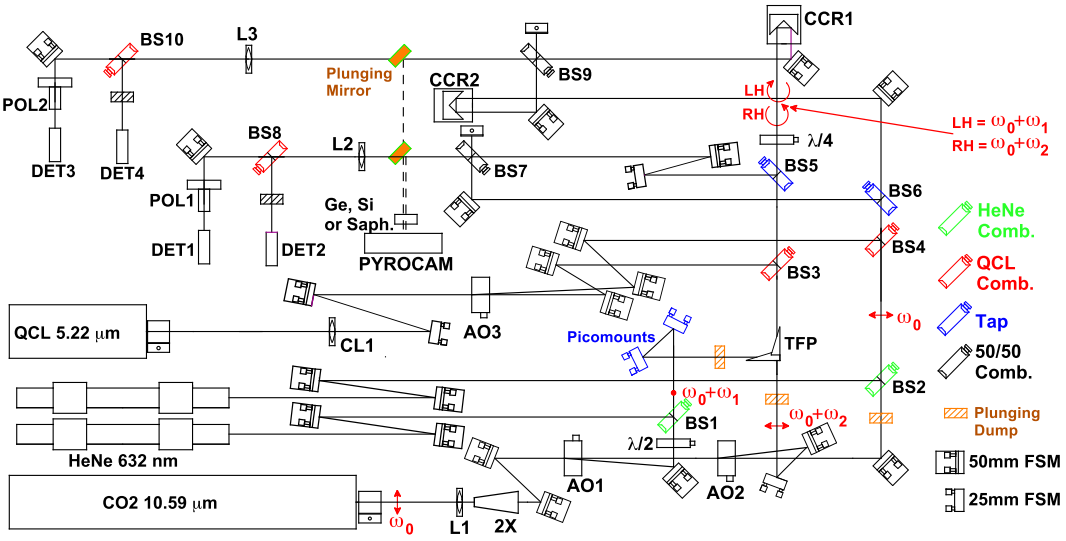

Figure 1. TIP prototype table layout for bench tests. Table dimensions are: 1.2 m × 2.4 m. HeNe lasers are for alignment purposes only. Tap = ZnSe beamsplitter (45° AOI, $R \approx 5\%$, $T \approx 95\%$, at 5.42 and 10.59 μm), AO1, AO2, AO3 = germanium acousto-optic modulator 40, 44, 40 MHz, $\lambda/2$ = CdS half-wave plate, HeNe Comb. = ZnSe beam combiner (45° AOI, $R \approx 99\%$ at 632 nm, $T \approx 99\%$ at 10.59 μm), TFP = ZnSe thin film polarizer, $\lambda/4$ = 10.59 μm CdS quarter-wave plate, QCL Comb. = ZnSe beam combiner (45° AOI, $R \approx 99\%$ at 5.42 μm, $T \approx 99\%$ at 10.59 μm and 632 nm), 50/50 Comb ., = ZnSe beamsplitter (45° AOI, $R \approx 50\%$, $T \approx 50\%$ at 5.42, 10.59 μm and 632 nm), DET1, DET2, DET3, DET4 = HgCdTe PV detectors, Pol1, Pol2 = 10.59 μm ZnSe Brewster Angle Based Polarizer, FSM = front surface mirrors, $L1 = 25.4$ cm FL ZnSe lens, $L2$ and $L3 = 50$ cm FL ZnSe lens, CL1 = −1.2 m FL CaF2 cylindrical lens, Pyrocam = Ophir Pyrocam^{TM} beam profiler.

development of a feedback alignment system on a long 120 m beam path then TIP prototype measurements with feedback alignment on the 120 m beam path. In section 2, a detailed description of the TIP prototype design, bench test results and measurements of density in a pulsed radio frequency (RF) plasma device are presented. In the following section 3 a description of the long beam path and basic feedback alignment strategy/technology are presented. In section 4 measurements with the TIP prototype on the full beam path with feedback alignment are discussed, where it is shown that the TIP prototype is capable of meeting ITER's measurement requirements.

2. Iter TIP prototype preliminary layout and bench testing

The work presented in this section describes the initial testing of an ITER TIP prototype and characterization of the performance. This section is restricted to bench tests in which, with the exception of measurements of an RF plasma device, the system is contained entirely on a single optical table in a temperature regulated enclosure. The following sections extend the testing to a long beam path complete with feedback alignment.

2.1. Components, optical table layout and principle of operation

The TIP prototype optical table layout used for bench testing is shown in figure 1. The bench test layout and principle of operation is very similar to that presented in [4] and allows a heterodyne phase measurement to be made for determination of both the interferometric phase shift and Faraday rotation, analogous to techniques developed using far infrared lasers on Rijnhuizen Tokamak Project [18, 19], Madison symmetric torus (MST) [20–22], and more recently CO_2 lasers on large helical device, [12] and DIII-D [13]. Two key elements that were not presented in [4], but that appear in figure 1, include the 5.22 μm QCL (discussed in section 2.1.2) and the Picomotor^{TM} mounts and Pyrocam^{TM} beam profiler to enable precision alignment (discussed in section 2.1.3).

The basic principle of operation is that radiation from a single 10.59 μm CO_2 laser (frequency $\omega_0 = 2.8 \times 10^{13}$ Hz) is used to create both right-handed (RH) and left-handed (LH) circularly polarized radiation with a difference frequency of $\delta\omega = (\omega_2 - \omega_1) =$ 4 MHz, (where $\omega_1 = 40$ MHz and $\omega_2 = 44$ MHz) as well as horizontally polarized light with frequency ω_o (reference leg) [10, 11]. The drive for the AO cells is adjusted such that the incident beam is split into approximately equal amplitude components at ω_0, $\omega_0 + \omega_1$, and $\omega_0 + \omega_2$ with linear polarization in the plane of the paper. The $\omega_0 + \omega_1$ component is then passed through a CdS $\lambda/2$ wave plate and its polarization is rotated by 90°. The two separate frequency ($\omega_0 + \omega_1$, and $\omega_0 + \omega_2$), orthogonally polarized beams are then re-combined using a ZnSe thin film polarizer/combiner (TFP) operating at Brewster's angle. Immediately after being combined at the TFP, this composite beam is split (BS5) and a fraction is used to form the optical local oscillator (LO). After being combined with a fraction of

the reference leg power at frequency ω_o, the combined beams are sent through a polarizer at 45° and to a reference detector (Detector 1). Detector 1 signals at frequencies $(\omega_2 - \omega_1)$ and ω_1 are essentially used to form the LO waveforms for demodulation of the Faraday rotation and interferometry phase shifts respectively. Demodulation with respect to this optical LO removes any vibration that enters when the beams are separate—something which would otherwise dominate the polarimeter phase shifts. After a portion of the plasma leg is split by BS5, the remaining composite beam is then passed through a CdS $\lambda/4$ wave plate with its axis at 45° with respect the polarization vector of each frequency component forming the superimposed counter-rotating LH and RH waves at $\omega_0 + \omega_1$, and $\omega_0 + \omega_2$ respectively (i.e. rotating linearly polarized wave at $\delta\omega/2$). The RH and LH beams are then sent to CCR1 (essentially forming the end of the 'plasma leg'), then through a polarizer and to a separate detector (Detector 3) after being combined again with a separate reference leg at the unshifted frequency ω_o that is fixed to be the same path length. Separation of the plasma and vibration induced phase shifts in the interferometer measurement is accomplished by using a second co-linear QCL laser based interferometer operating at 5.22 μm where the LO signal is taken at 40 MHz from Detector 2 and the IF signal is from Detector 4—so called vibration compensated two-color interferometry.

2.1.1. Table enclosure. Due to the sheer number of optical components and extremely sensitive alignment, controlling the TIP optical table environment is critical. To do this, an optical table enclosure was constructed that seats directly on the optical table surface and is 30 cm tall. The wall material is Arboron™ a melamine-faced solid phenolic laminate and the inside of each panel is covered with an anodized aluminum sheeting to further prevent any laser damage. The side-panels are bolted to an aluminum frame and the removable top panels are magnetically seated for access. The temperature in the optical table enclosure is maintained by a series of 5 watt heating elements controlled by a PID temperature controller. The temperature controller takes in the signals from four separate thermocouples placed at different locations in the enclosure, averages them, and turns the heaters on as needed to regulate the temperature. The system response is slow with approximately 2 °C change per 30–60 min. The principle of operation is that the enclosure is set to 25.5 °C which is approximately 1°−2° above the maximum ambient room temperature and the room temperature is then controlled by the building HVAC system (the thermostat for which is located in the actual TIP prototype room).

2.1.2. Lasers. The original TIP baseline design was based on a carbon monoxide and CO_2 laser at 5.42 and 10.59 μm respectively [2, 4]. The TIP prototype, however, takes advantage of recent laser advances and is based on a QCL and

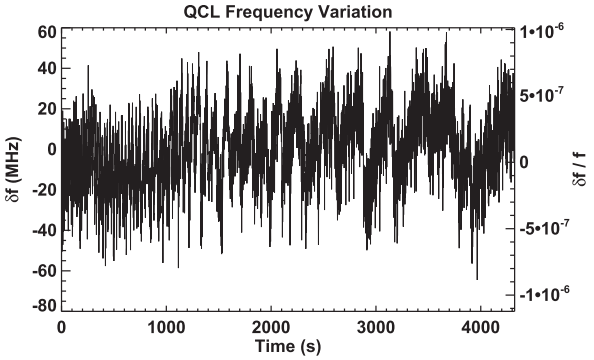

Figure 2. QCL frequency variation about center 5.22 μm wavelength.

CO_2 laser operating at a similar wavelength combination of 5.22 and 10.59 μm. These lasers are described below.

QCLs are a promising new development in the mid-infrared laser field. For the TIP prototype, a 5.22 μm Daylight Solutions Unicorn™ fixed wavelength QCL was chosen. The QCL used is for the shorter vibration compensation wavelength and chosen as a replacement for the originally proposed CO laser operating at 5.42 μm. The change was made after operational experience with a CO laser proved it to be extremely challenging, due to both power and wavelength stability issues, and it was realized few vendors could supply a suitable CO laser. The QCL employed here is a turn-key 150 mW single mode, stable laser suitable for interferometry.

One key requirement for the TIP two-color interferometer measurement is linewidth/wavelength stability. Since the standard analysis procedure has a fixed wavelength ratio for vibration compensation, any wavelength variation shows up directly as an error in density measurements, the magnitude of which is dependent on the vibration. To keep the error contribution of the wavelength ratio $(R_\lambda = \lambda_{CO_2}/\lambda_{QCL})$ determination for the interferometer comparable to that of the phase demodulation process requires an accuracy of the order 10^{-5}. For 2 mm of equivalent motion, and $\delta R_\lambda/R_\lambda = 10^{-5}$, the error introduced in the density integral determination is equivalent to $\approx 1°$. of error in the CO_2 interferometer phase measurement [4]. The wavelength stability of the QCL was measured using a Bristol Instruments wavemeter over 4300 s and is presented in figure 2, where it is found to be $\delta f/f < 10^{-6}$.

Due to the nature of the QCL emission cavity, the beam expansion is astigmatic resulting in a Gaussian, but asymmetric beam profile. The measured 2D beam profile 1 m from the laser head is shown in figure 3 along with 1D and 2D Gaussian fits. The Gaussian beam radii as a function of distance from the laser head are shown in figure 3(d). Fortunately, the horizontal and vertical beam profiles have the same radius at a point outside of the laser head ($D = 0.487$ m) so a cylindrical lens can be placed at that location to match the expansion of the beams. The calculated result is shown overlaid 3 as a green dashed line, where the beam radii are shown with a focal length

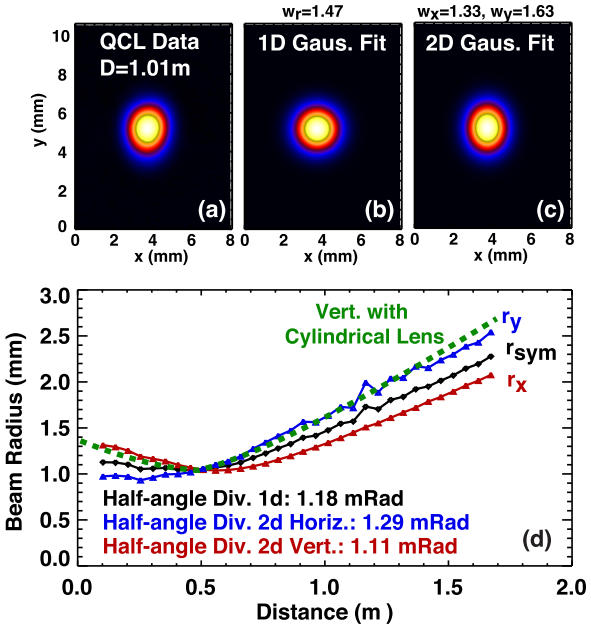

Figure 3. 5.22 μm QCL 2D structure at 1 m from head. (a) Data, (b) symmetric Gaussian fit, (c) asymmetric Gaussian fit. (d) QCL beam radius assuming symmetric Gaussian (r_{sym}), and asymmetric Gaussian (r_x, r_y).

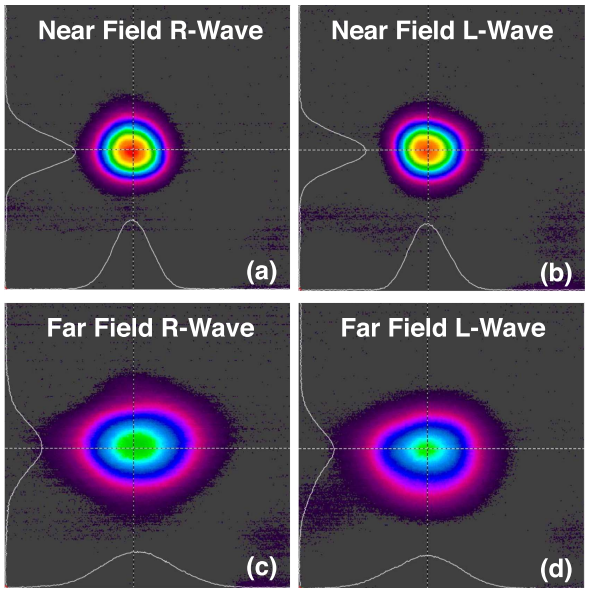

Figure 4. Measured beam profiles during the alignment process of the CO_2 *R* and *L* wave in the near field (a) and (b), as well as far field (c) and (d). Each panel is 25 mm× 25 mm.

$F = -1.2$ m cylindrical lens placed at $D = 0.487$ m. After that distance, the QCL beam is extremely symmetric and Gaussian with a uniform divergence. This has been implemented with a CaF2 cylindrical lens as shown in the optical table layout figure 1

The CO_2 laser used is an Infrared Instruments model IR-7-WS-GF-HP, which is a fixed grating, water cooled, heater stabilized, 10.59 μm, CO_2 laser with nominally 5–8 watts of output power. This is the same model laser used for 20+ years in the DIII-D two-color interferometer with excellent success and reliability. Measurements similar to those in figure 3 for the QCL show the CO_2 beam is very symmetric and well fit by a symmetric Gaussian with a divergence found to be approximately 3.3× that of the QCL (divergence $CO_2 = 4.3$ mRad).

2.1.3. Picomotor™ based co-alignment. A major factor in TIP performance is the degree to which the 10.59 μm *R* and *L* waves and to a lesser extent, the vibration compensation 5.22 μm QCL beams can be made collinear. In previous systems, this has been accomplished using a manual process in which the beams are imaged on a fluorescing plate or liquid crystal sheet in the near and far field and a set of mirrors are adjusted iteratively to align the different beams to one another. This type of process is likely not precise enough for the TIP measurement where estimates indicate the *R* and *L* wave beam centerlines must be overlapping to better than a few hundred microns in the ITER vessel to avoid contamination by density gradients and corresponding differences in the interferometric phase shifts of the non-collinear beams. Additionally, that process does not lend itself to automation and requires manual insertion of targets and blockers on a very populated optical table, greatly increasing the risk of bumping and misaligning optics.

To overcome the limitations of the manual alignment process, a remote controlled mirror mount and beam profiling camera based approach was developed. In this approach, plunging mirrors (figure 1) are used to direct the optical LO beams or the final beam combiner beams to a beam profiling camera (Ophir Pyrocam™) forming the near and far field check locations. At the plunging mirror positions, all beams (10.59 μm *R* and *L* plasma leg, horizontal reference leg, 5.22 μm plasma and reference legs, 0.632 μm alignment plasma and reference legs) are present. The beams can be blocked using remote beam blocks or filtered using germanium (5.22 and 10.59 μm only), sapphire (5.22 and 0.632 μm only), or unfiltered. Picomotor™ mirror mounts, which are a remote controlled type of inertia based piezo-electric actuator, are then used to align the various beams. For testing purposes, remote actuators were only used for the actual *R* and *L* wave alignment and are shown in figure 1, where they act on the vertical polarization (before it is turned into circular polarization by the half-wave plate). The Picomotor™ mirrors are used to iteratively adjust the near and far field on the beam profiler until the *R* and *L* wave beams are co-linear, i.e. one stays fixed. Near and far field measurements from the beam profiler of the *R* and *L* wave are shown in figure 4.

Once a careful alignment process like this has been carried out, the relative *R* and *L* wave as well as 5.22–10.59 μm alignment has been observed to be extremely stable, influenced only by large variations in either enclosure temperature ($> \pm 2$ °C) or a laser specific problem such as a change in AO cell water flow and/or power levels.

Future implementations of this approach will utilize remote mount adjustment of all beams. In this implementation, the power previously being thrown away from both the optical LO and final 50/50 beam combiners can be used. By using the previously dumped power, the plunging mirror/dump selects either the near-field (red) or far-field (blue) beams to a single beam profiler without interrupting the beams used for the actual interferometer and polarimeter measurement. Such an approach has several attractive characteristics: utilizes a single beam profiler, Picomotor™ mounts allow precise remote adjustment, can be continuously monitored without interrupting measurement and lends itself to automation.

2.1.4. Phase measurement software. Phase measurements for the TIP system are made using a demodulator developed by Palomar Scientific Instruments specifically for this project. The details of the TIP digital phase demodulator (DPD) will be described in a separate paper, however, a summary is presented here. The DPD is built around a modern FPGA interfaced to four high-speed ADCs. The DPD measures the phase shift of three intermediate frequency signals (4, 40, and 44 MHz) from two different CO_2 laser detectors and a 40 MHz signal from two different QCL detectors on the optics table with a demonstrated instrumental phase resolution of $\delta\phi < 0.01$. with 500 kHz useable bandwidth and $\delta\phi < 0.002°$. with 1 kHz bandwidth. The unit is packaged in a rack mounted case, shown in figure 5(a).

Phase measurements are made in real time and streamed to the TIP laboratory computer for viewing using software written in the C++ language. A screenshot of the main operator panel is shown in figure 5(b). The panel provides a graph of the phase and magnitude of each of the three frequencies and four channels. One channel/frequency measurement is shown at a time for clarity. The software also displays some statistical analysis measurements including mean and variance. This is useful while making adjustments to the TIP system as it provides immediate feedback. The software is also capable of displaying a real-time spectral analysis of the phase signals.

Data from the DPD can be streamed to the hard-drive of the computer for later analysis at both low (50 kS s^{-1}) and high (1 MS s^{-1}) bandwidth. As will be discussed in the following sections, shots as long as 1500 s have been acquired in order to test the long-term stability of the interferometer.

2.2. Bench test results

The following section discusses TIP prototype bench tests carried out with the goal of characterizing noise floors as well as overcoming major issues before directing the system along the long beam path.

2.2.1. Path length matching between interferometer legs. In the initial phases of the TIP bench testing, it was unknown how well the reference and plasma leg beam paths had to be matched for low-noise interferometry measurements. In principle, the coherence length of the lasers sets an upper bound on this (up to 100 m) but experience on the DIII-D system indicated some lasers required better than centimeter matching for low-noise density measurements. To test this, the reference and plasma legs were intentionally mismatched and the phase noise spectrum was measured. The results for 20 cm mismatch are shown in figure 6. It was found that the

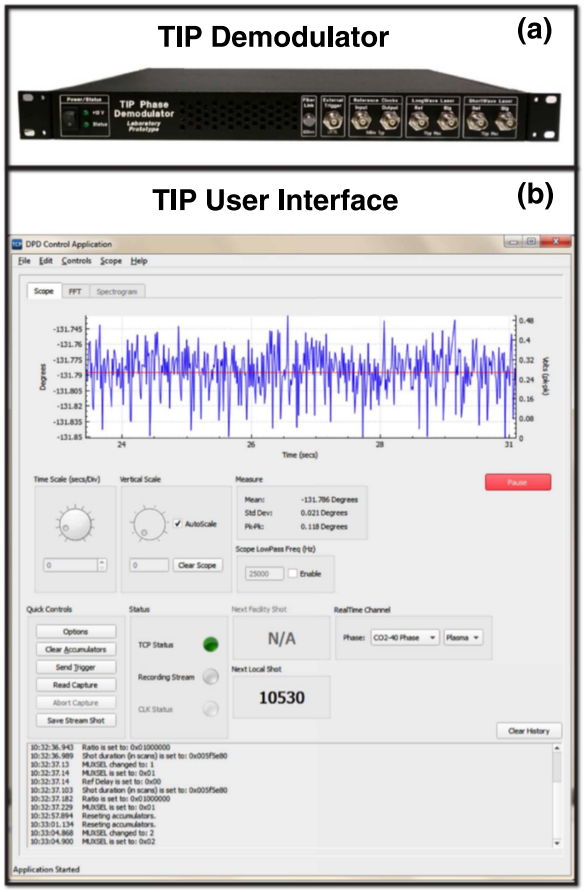

Figure 5. (a) TIP digital phase demodulator hardware. (b) Screenshot of the main operator panel of DPD software.

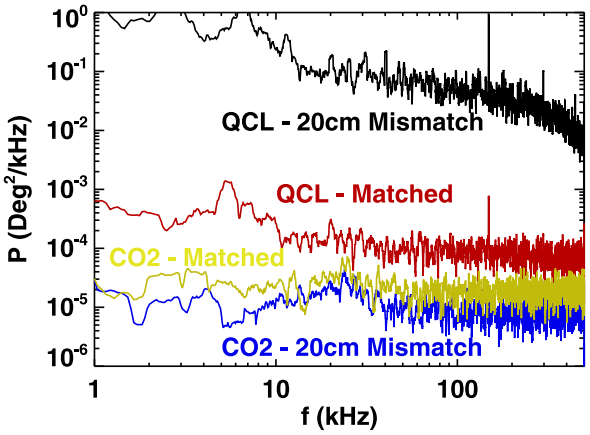

Figure 6. Path length matching impact on phase noise.

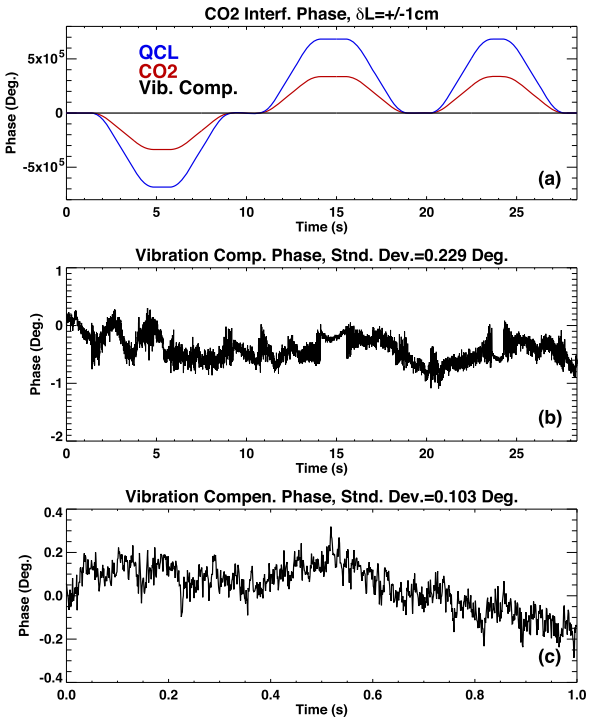

Figure 7. Interferometer phase during plasma leg CCR motion. (a) QCL, CO_2 and vibration compensated phase. (b) Vibration compensated phase only. (c) Vibration compensated phase over 1 s interval.

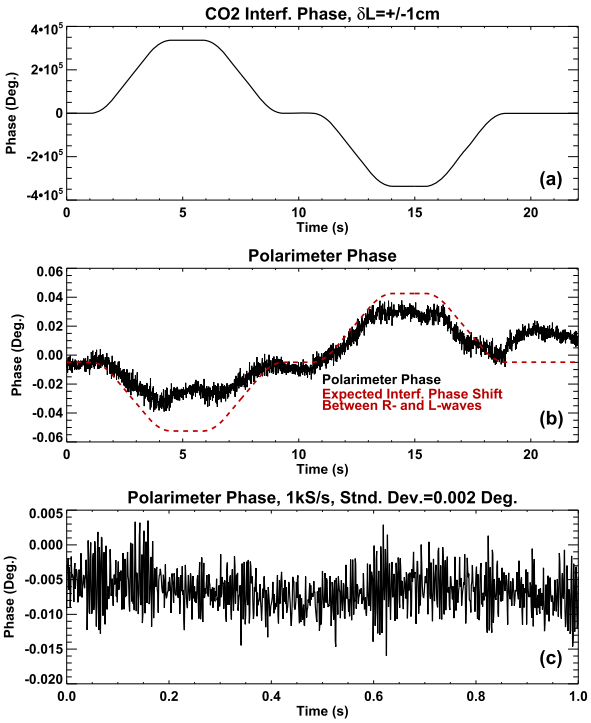

Figure 8. CO_2 interferometer and polarimeter phase shifts during ± 5 mm CCR motion. (a) Uncompensated CO_2 inteferometer phase. (b) Polarimeter phase and expected phase shift interferometric phase shift between R and L waves. (c) Polarimeter phase over 1 s interval.

20 cm path length mismatch has a negligible impact on CO_2 laser phase noise but has a severe impact on QCL phase noise. For a 20 cm mismatch, the noise can be several orders of magnitude larger. When matched, the phase noise is comparable between the two lasers but slightly larger for the QCL. Finer scale measurements show centimeter level mismatches can make a measurable impact on QCL phase noise. This fact is actually used as a means for precise path length matching and will be discussed further in section 4.1.1. For the rest of the tests in this section, the path lengths are matched to <1 cm. One practical implication of broadband phase noise, like that in figure 6, is the impact on high frequency fluctuation measurements. Fortunately, vibration compensation is not necessary above $\approx$10 kHz so CO_2 phase measurements (which are not as sensitive to path length matching) alone can be used for fluctuation analysis. Additionally, if this proves to be an issue with future systems, QCLs with approximately an order of magnitude narrower linewidth are available commercially.

2.2.2. CCR jogs and vibration compensation. One very sensitive test of the TIP functionality is introducing intentional motion of one of the CCRs to simulate large-scale vibration and relative path length changes between the reference and plasma legs. The two-color system should be able to compensate for the motion and the polarimeter system should be relatively insensitive to the motion. Figures 7 and 8 show exactly this behavior. In these tests, the plasma leg CCR is displaced periodically back and forth ± 5 mm introducing $\delta L = \pm$ 1 cm path length changes. Figure 7(a) shows the corresponding QCL, CO_2 laser, and vibration compensated phases, where even in the presence of 10^5 degree phase changes, the vibration compensated phase noise is $\delta\phi_{\rm int} = 0.2^\circ$ over the 30 s interval and $\delta\phi_{\rm int} = 0.1^\circ$ over a 1 s interval. For reference, the ITER specification is $\delta\phi_{\rm int} = 10^\circ$. Additionally, the enhanced noise that is apparent during the actual CCR motion (periods of rapid phase change in figure 7(a)) were found to be due to a small non-deterministic delay between FPGA digitizer channels. Since these data were taken, a solution for this was implemented, and the upgraded version without this artifact is used in measurements with the full beam path presented in section 4.

The polarimeter measurements show equally encouraging results in the presence of ± 1 cm path length changes and are given in figures 8(b) and (c). The corresponding CO_2 phase is shown in figure 8(a). The polarimeter phase in figure 8(b) shows periodic small amplitude excursions that appear synchronized with the CCR motion. This is actually an expected effect and is due to the interferometric phase shift difference between the R and L wave resulting from their 4 MHz frequency difference. The expected phase shift derived from the CO_2 phase measurement in panel figure 8(a) is overlaid as a dashed red line in figure 8(b). If desired, this could be removed from the polarimeter phase measurement. Over a 1 s interval (figure 8(c)), the polarimeter

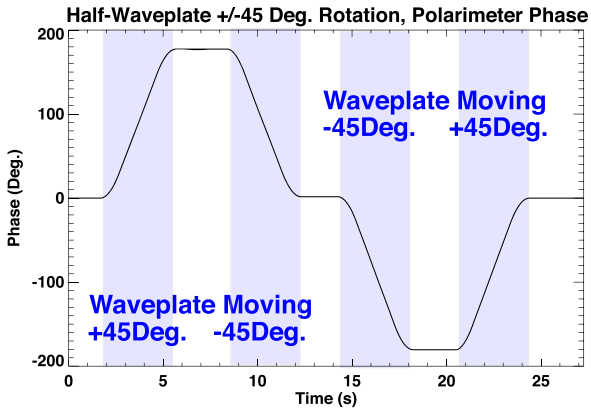

Figure 9. Polarimeter phase during ±45° half-wave plate rotations.

phase noise is extremely small at $\delta\phi_{\rm pol} = 0.002°$. For reference, the ITER specification is $\delta\phi_{\rm pol} = 0.1°$.

2.2.3. Wave plate simulated Faraday rotation. In addition to tests verifying the relative immunity to path length changes and vibration, the polarimeter is tested by rotation of a half-wave plate in place of a magnetized plasma to simulate Faraday rotation. This is a standard technique for calibrating *R* and *L*-wave based polarimeters such as this and is routinely employed on MST and other devices [20, 23]. For every degree of half-wave plate rotation, the polarimeter phase shift should be 4°. Figure 9 shows polarimeter data taken as a 10.59 μm half-wave plate is rotated in the beam path. At every 45° rotation, the polarimeter phase clearly changes by 180° and returns to zero when the wave plate returns to its original position, confirming the polarimeter is functioning as expected. Future work will use this effect to generate a precise polarimeter phase to Faraday rotation angle calibration by introducing a calibrated wave plate rotation and recording the phase change. This may be required to account for any elliptization of the *R* and *L* waves introduced over time through coating of in-vessel optics, optical component degradation, etc.

2.2.4. Long-timescale interferometer and polarimeter measurements (1000 s). Some discharges in ITER are expected to last up to 1000 s so an important test of the TIP system involves acquiring data for 1000+ seconds and checking the long timescale stability of the system. Results from a 1000 s data acquisition of interferometer and polarimeter data are shown in figure 10. Interferometer data (figure 10(a)) show very low noise $\delta\phi_{\rm int} = 0.65°$ over the entire window with a small steady drift of ≈1.8°. Over the same window, the polarimeter (figure 10(b)) phase noise is $\delta\phi_{\rm pol} = 0.02°$ with a small drift of approximately 0.07°.

While the combined polarimeter and interferometer measurements (shown in figure 10) made using a single detector are able to meet ITER's density measurement requirements, polarimeter phase noise can be improved significantly by extracting the 4 MHz polarimeter signal before the plasma leg is mixed with the reference leg. In practice, this

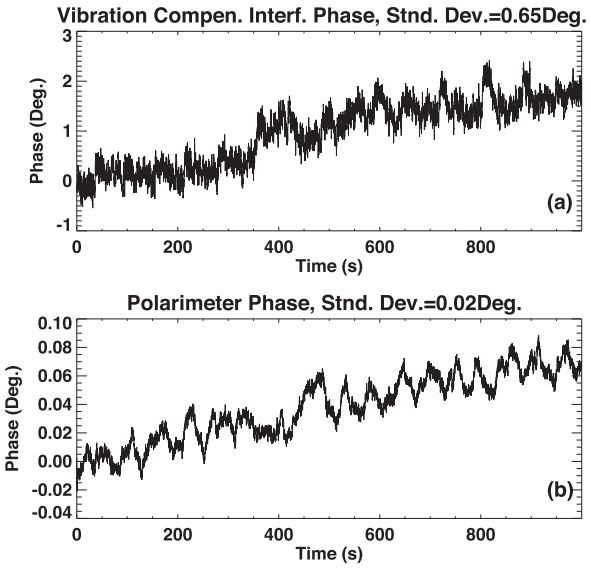

Figure 10. 1000 s measurement of (a) interferometer and (b) polarimeter noise floors.

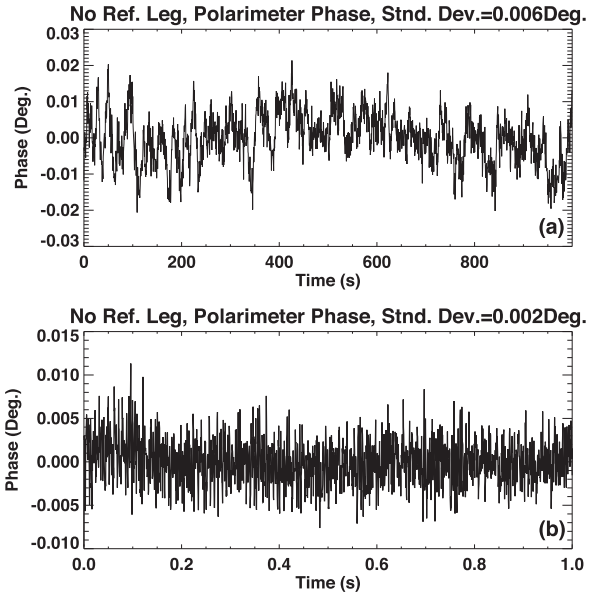

Figure 11. Polarimeter phase noise with the CO_2 reference leg blocked. Data are shown over (a) 1000 s and (b) 1 s intervals.

will be carried out by splitting a portion of the plasma leg off after it returns to the table and sending it to its own dedicated detector. The remainder will then be sent to a beam combiner to be combined with the reference leg for extraction of the 40 and 44 MHz interferometer phase shifts. To simulate this for testing purposes, the reference leg is simply blocked. The results of a 1000 s data acquisition with the CO_2 reference leg blocked are show in figure 11 where extremely low phase noise of $\delta\phi_{\rm pol} = 0.006°$ and no drift is found. Over a 1 s interval, the noise is even lower at $\delta\phi_{\rm pol} = 0.002°$.

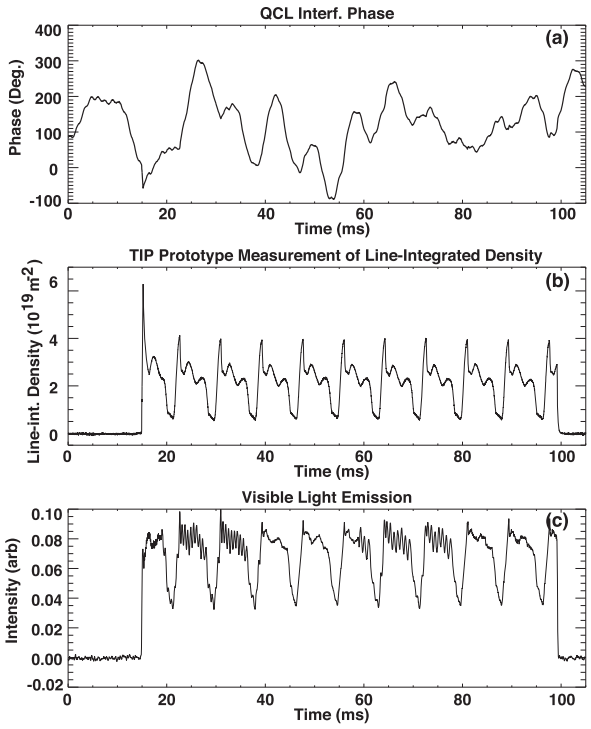

Figure 12. TIP prototype measurements of an RF plasma device. (a) QCL phase shift during pulse. (b) Vibration compensated measurement of line-integrated density. (c) Visible light emission.

2.3. TIP prototype measurements of a RF plasma device

In order to demonstrate the TIP prototype's ability to measure actual plasma density before moving to long beam path studies, the plasma leg was routed through, a pulsed RF plasma device that has been used for previous interferometer testing (fiber optic two-color, microwave and CO_2 dispersion) [24, 25]. The device is located on an adjacent table and the plasma is powered by an 8 kW self-tuning RF plasma source (Advanced Energy PDX-8000). The cylindrical argon test plasmas have neutral fill pressures of 50–300 mTorr, duration < 200 ms, peak electron densities of order 10^{20} m^{-3}, length and diameter of $L_{\text{plasma}} \approx 0.5$ m and $D_{\text{plasma}} \approx 0.08$ m, as well as an axial magnetic field of $B < 200$ G. The interferometer beam path makes two axial passes through the plasma.

The measured uncompensated QCL phase and line-integrated density from a typical discharge are shown in figures 12(a) and (b) respectively. The discharge shown initiates near $t \approx 15$ ms and terminates at $t \approx 98$ ms. The majority of the vibration comes from vacuum pumps attached to the plasma chamber and same table as the mirrors and corner cube. The peak vibration over the interval shown is roughly 5 μm corresponding to one fringe of the 5.22 μm beam, while the peak measured line-integrated density is $nL = 6 \times 10^{19}$ m^{-2}. The interferometer density resolution as measured before the plasma start is extremely good at $\delta nL = 3.5 \times 10^{17}$ m^{-2} with 50 kHz bandwidth, corresponding to an equivalent of $\delta\phi_{\text{int}} = 0.45°$. Additionally, the system's ability to track rapid density changes is shown at each of the periodic drops in density spaced approximately 10 ms apart. These are the result of reflected power/tuning oscillations in the plasma source and are also apparent in the visible light emission shown in figure 12(c). These data represent the first measurement of a plasma by a combined CO_2/QCL two-color interferometer and polarimeter with a density resolution an order of magnitude better than that required for ITER.

3. Full-scale beam path and feedback alignment

The ITER TIP will consist of five chords, with round trip path lengths from approximately 110 to 120 m. To simulate the expected impact of motion on the TIP measurement, the required aperture sizes and our ability to keep the diagnostic aligned using a feedback alignment system, a full-scale mockup beam path was created that mimics the distances and motions expected on the longest TIP chord. The round trip laboratory beam path is 120 m where the *plasma* and *reference* legs are shown in red and blue respectively in figure 13.

3.1. Beam path components, layout and motion simulation

A zoomed in region of figure 13 can be seen in figure 14, where several of the primary components and locations have been identified. In the lab beam path, both the plasma and reference legs leave the TIP optical table and travel through the ceiling. The reference leg (blue) travels 60 m to a high-quality protected silver coated 125 mm clear-aperture retro-reflector after hitting a 20 m focal length mirror located 40 m from the optical table. The beam then returns along the same general path on the same set of mirrors, except slightly skew due to the focusing mirror. All mirrors on the reference leg are 150 mm diameter protected silver coated front surface mirrors. The plasma leg is meant to simulate the beam going to/from ITER and through the actual device. The plasma leg travels approximately 30 m before being directed to the wall of the beam path lab. All components along the wall (after the location labeled 'Bioshield') are enclosed in a common plexiglass enclosure (not shown). The components mounted to the wall are meant to simulate the ITER interspace area, equatorial port nine (EP9), and the actual vacuum vessel path to the retroreflector [4]. The simulated EP9 consists of two turning mirrors, a carbon fiber tube, and a 88.9 mm diameter barium fluoride (BaF_2) window. The retroreflector is designed to have the incoming and return beams slightly skew as discussed below. To maintain R and L wave integrity, all larger 90° turning mirrors on the plasma beam path are custom silicon 150 mm diameter front surface mirrors with a coating designed to impart no phase shift between S and P polarization components. All beam paths are enclosed by 150 mm diameter aluminum piping.

3.1.1. Retroreflector. As mentioned above, the current TIP design uses novel slightly 'imperfect' retroreflector with two of the facets tilted from their nominal position. The goal of

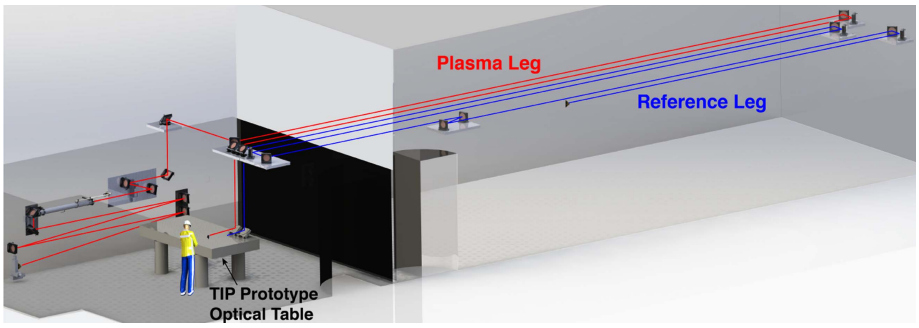

Figure 13. CAD model of the full-scale TIP prototype. All ceiling mirrors are housed in aluminum enclosures and beams travel through 150 mm diameter aluminum piping (not shown).

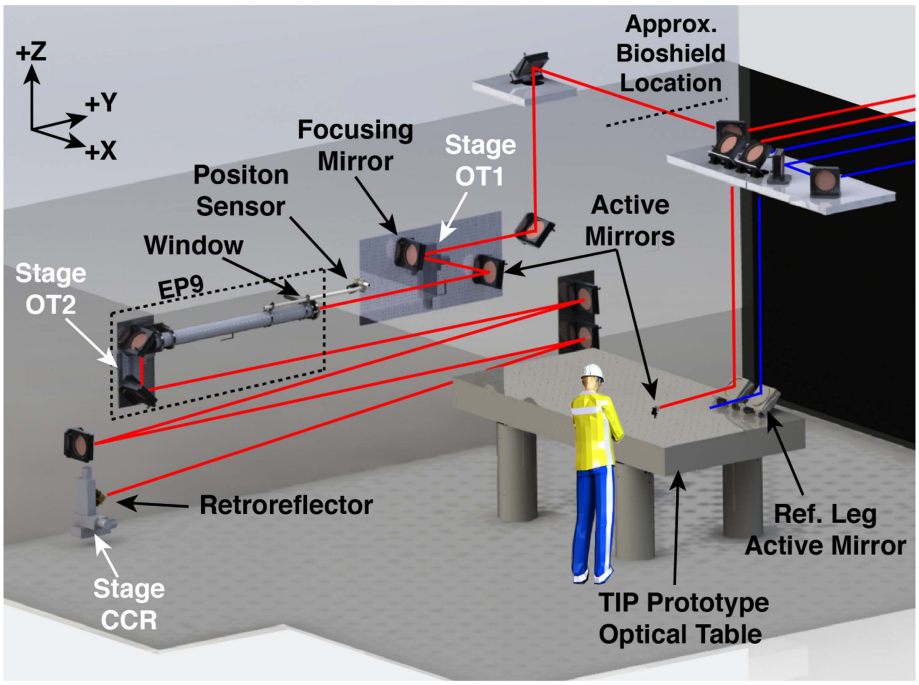

Figure 14. Enlarged region of figure 13 showing several key components of the extended beam path.

the facet tilt is to make the return beam cross the outgoing beam at the ITER first wall penetration (or nearby) thereby reducing the required size of the hole, something which is advantageous from a standpoint of erosion, deposition and neutron shielding. This design was incorporated into the full-scale mockup beam path and results in a 0.131° angle between the incoming and outgoing beams. The mockup retroreflector is fully adjustable as each square mirror is placed on its own kinematic mount. This design allows not only making a 'perfect' retroreflector but intentional distortions to investigate the TIP prototype's ability to respond to situations such as those encountered during heating of the ITER in-vessel retroreflectors.

3.1.2. Beam position monitoring (for passive analysis). Both for passive initial alignment and as the translations stages are exercised through their range of motion, some monitor of the laser beam position on the actual steering mirrors is required. All mirrors besides those in the plexiglass enclosure are not easily accessible and remote viewing is required. To accomplish this task, an inexpensive, multi-camera, networked security monitoring set is employed. The primary mirrors and apertures are outfitted with small cameras and the beam position on each mirror can be clearly monitored.

3.1.3. Motion simulation in mockup beam path. The simulation of expected motion that will be experienced by the TIP diagnostic is carried out by using a set of seven translation stages (one X, Y, Z and two X, Y combinations) mounted at three separate key locations in the prototype beam path. Each stage is highlighted in figure 14 and is capable of approximately 50 mm of motion along each axis. In figure 14, the movable stages are identified as OT1, OT2, and corner

Table 1. Radial, toroidal, and vertical motion on the outboard midplane of an ITER port plug during different scenarios (taken from [26]) considered in this work and corresponding motion on translation stages. Note, all positions are with respect to Ambient at which the initial alignment is carried out.

	Ops (mm)	Bake (mm)
ITER radial	13.23	30.54
ITER toroidal	0.002	0.003
ITER vertical	10.44	27.05
EP9/OT2 stage—*Y*	13.23	30.54
EP9/OT2 stage—*Z*	10.44	27.05
CCR stage—*X*	6.62	15.27
CCR stage—*Y*	−11.46	26.45
CCR stage—*Z*	10.44	27.05

cube reflector (CCR). Stages OT1 and OT2 are capable of *X* and *Y* motion whereas the CCR stage is capable of *X*, *Y*, *Z* motion. The combination of these stages allows simulation of several different scenarios including those in which optics are attached or not to the simulated EP9. For scenarios simulating the case where final steering optics are rigidly attached to EP9, stages OT1 and OT2 move in a synchronized manner. Motion control software was developed for testing of the feedback alignment response to simulated ITER motion. Key positions to simulate the distinct temperature states of the ITER vessel were identified and named: HOME—the position of all axes at the home position, found using mechanical limit switched mounted on the stages. AMBIENT—the position corresponding to the vessel at installation and maintenance conditions. BAKE—the position corresponding to the vessel during bake. OPS—the position corresponding to the vessel at operating conditions.

The actual predicted ITER displacements are given in the first three rows of table 1 and the corresponding displacements of each stage for the various scenarios are given in table 1, where the radial, toroidal and vertical motion of the outboard ITER midplane was decomposed into the stage *XYZ* coordinate system. First, all axes are homed then moved to AMBIENT position. The optics and electronics are aligned and tuned at this position. The stages are then moved to BAKE position at specified rate to be determined, held for period, and then moved to OPS position. Once at OPS position, small perturbations of specified amplitude and period can be executed for testing and refining feedback alignment strategies. Beam line positions at the various bake cycle stages (Ambient, Ops, Bake) on the ITER outboard midplane are taken from [26] and decomposed into corresponding motion on translation stages. The values are repeated in table 1.

3.2. Feedback alignment components and design

A diagram showing the feedback alignment strategy is given in figure 15 for both the plasma (figure 15(a)) and reference (figure 15(b)) legs. The plasma leg has two active mirrors controlled by position sensors placed near the EP9 window and back on the optical table. These position sensors control

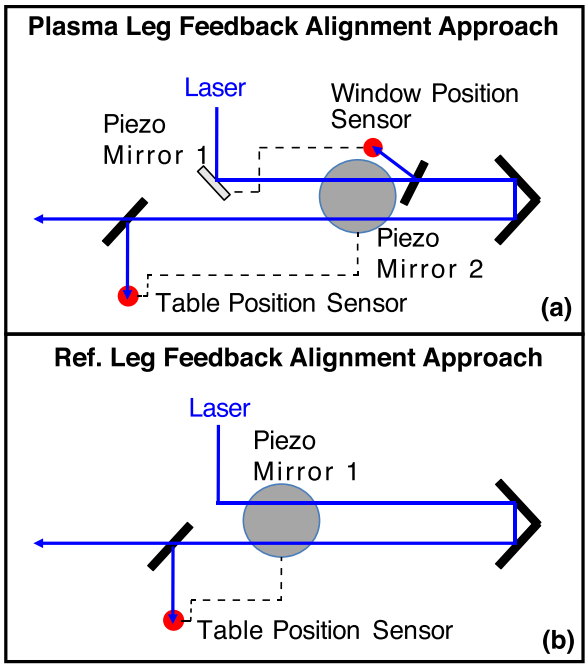

Figure 15. Diagram showing feedback alignment approach for (a) plasma leg and (b) reference leg. Dashed line indicates which position sensors are used to control a corresponding piezo tip/tilt platform.

active mirrors placed on the optical table and near EP9 respectively. The basic idea is that the first active mirror keeps the beam fixed at the center of the EP9 window and the second active mirror keeps the plasma leg beam fixed after returning to the TIP optical table. The reference leg will experience less motion and uses a single active mirror to keep the beam fixed after returning to the optical table. All feedback alignment in this work utilizes the co-linear visible alignment laser.

To help reduce the number of transmissive components to only those that are essential, the mockup plasma leg beam path leverages the BaF_2 window to sample the beam for position sensing. The BaF_2 window at the nominal EP9 closure plate location is tilted at $\approx 5^\circ$ such that some fraction of the incident beam is reflected and is sent to a position sensing element (Thorlabs PDP90A). At 5° angle of incidence, the reflected 637 nm alignment laser power fraction is approximately 4% Analogous to this, using the outer vacuum window is what is currently envisioned for the actual ITER TIP implementation. In all foreseeable scenarios where an attempt is made to keep the beam position fixed at the EP9 window, the position sensing element must move with the window. Without this constraint, it is far more difficult to guarantee that incoming beam always strikes the same position on the window.

The active mirror platforms used in the prototype beam path are Physik Instrumente models S-340 and S-330 which are 50 mm diameter and 25 mm diameter respectively piezo stack tip-tilt stages. The S-330 has been used on the DIII-D

CO_2 interferometer active feedback system for several years with no issues. In the prototype the S-340 stages are used for the larger mirrors in the system and the S-330 is used to steer the first active mirror on the plasma leg which is 50 mm × 50 mm square. The PI piezo stack tip/tilt platforms are particularly well suited to ITER operation in that they have long lifetimes, are very radiation resistant and can be made completely nonmagnetic. In long-term tests, problem-free use with total doses of 2 megagray has been found [27].

3.2.1. Feedback alignment control software. The feedback alignment control system is based on a standard PID controller approach to process the position sensor signals and provide drive signals for the piezo tip/tilt platforms The TIP prototype described here relies on three individual Thorlabs TPA101 controllers; two for the plasma leg and one for the reference leg. While each controller operates autonomously to maintain alignment on their respective position sensors, they are also supervised and adjusted using a software interface developed for this application on the TIP DAQ computer. Ultimately, for the actual ITER implementation, the feedback control hardware algorithms will be implemented on ITER approved FPGAs.

3.2.2. Failsafe alignment. The goal of the active feedback alignment controller is to maintain the beam position on the center of the position sensors. The controller responds to any motion of the beam away from center using a feedback loop to reposition the beam back to center. This requires that the beam remains on the sensor element at all times. Since the beam may at times be interrupted or accidentally steered off the detector completely, a method for re-locating the sensor after loss has been implemented. This comprises a failsafe alignment strategy.

A successful failsafe alignment strategy for the TIP systems has several challenges and features. One challenge is the fact the plasma leg requires two coupled feedback loops. Fortunately the window sensor loop is relatively insensitive to the table sensor loop (return beam). A key feature of the failsafe alignment system is that each feedback controller functions as independent finite state machines, the states of which depend on several external signals including the status of the interlocks and laser power thresholds. Under normal conditions both plasma leg controllers (named Window and table) operate in closed loop mode utilizing the PID control algorithm. While in closed loop state each controller routinely tests and stores the signal levels and the positions on the detector. As long as the signal is above a set threshold the beam is considered 'good'. If the beam is good and the positions on the detector are within some set distance from the center the *X* and *Y* outputs of the controller are stored as 'last good position'. These positions are utilized as holding positions if the beam is lost (falls below threshold). If either controller loses a beam, each controller goes into a hold state and sets its output to the last good position. Next the interlocks and beam powers (using power detectors on the table) are tested. If either of these signals is found to be bad then the controllers remain in the hold state until remedied. If the laser interlocks and beam powers are tested to be good then the system initiates a search routine. A test of the window sensor is first made. If the beam is bad then the window controller employs a spiral search algorithm to find the window detector using the visible laser. The origin of the spiral search is the last good beam position. The window controller repeats the spiral until the window is found. If the window beam is good then the table controller executes a spiral search algorithm to find the table detector. 'Found' is defined as the point when the total power on the detector is above some preset limit and the beam is returned to the center.

3.3. Feedback alignment testing

In general, the feedback alignment system has been observed to maintain alignment robustly for extended periods of time with minimal intervention and is an essential part of the TIP prototype.

3.3.1. Movement on optics through bake cycle. One of the tests of the feedback alignment system is checking the systems' ability to maintain alignment as the programmable stages move through a simulated bake cycle. This section presents camera measurements of beam positions and motion made for each scenario at the Ambient, Ops, and Bake positions. Camera data for the CCR, Window, 1st Wall and EP9 apertures are shown in figure 16. The beam positions for these data are overlaid as a series of circles, yellow for outgoing and blue for return. The cameras for the 'CCR' and 'Window' monitoring panels do not move with the stages, so one can compare the different frames to get an idea for how much motion is involved. This figure illustrates several key points. First, the feedback alignment system is able to maintain alignment through the simulated bake cycle. The figure also shows a persistent feature of almost all measurements—unless the CCR is intentionally distorted (discussed in the next section), the actual beam positions on the retroreflector change very little, even for large changes in intermediary optics. This is determined by the outgoing and return beam position on the optical table which is essentially fixed by the outgoing beam and placement of the return beam position sensor. Another key point is that the outgoing position on the window is well maintained by the feedback alignment system. Both of these are very encouraging since it means the system can be aligned at the Ambient position then brought to Ops temperatures without worrying about clipping or vignetting from edges of in-vessel optical components which were sized according to the current ITER design values (100 mm diameter in-vessel mirrors). As expected, motion on intermediary optics, near the mid point of the beam path is larger since those locations are further from positions being held fixed. A video file which shows the cycling from

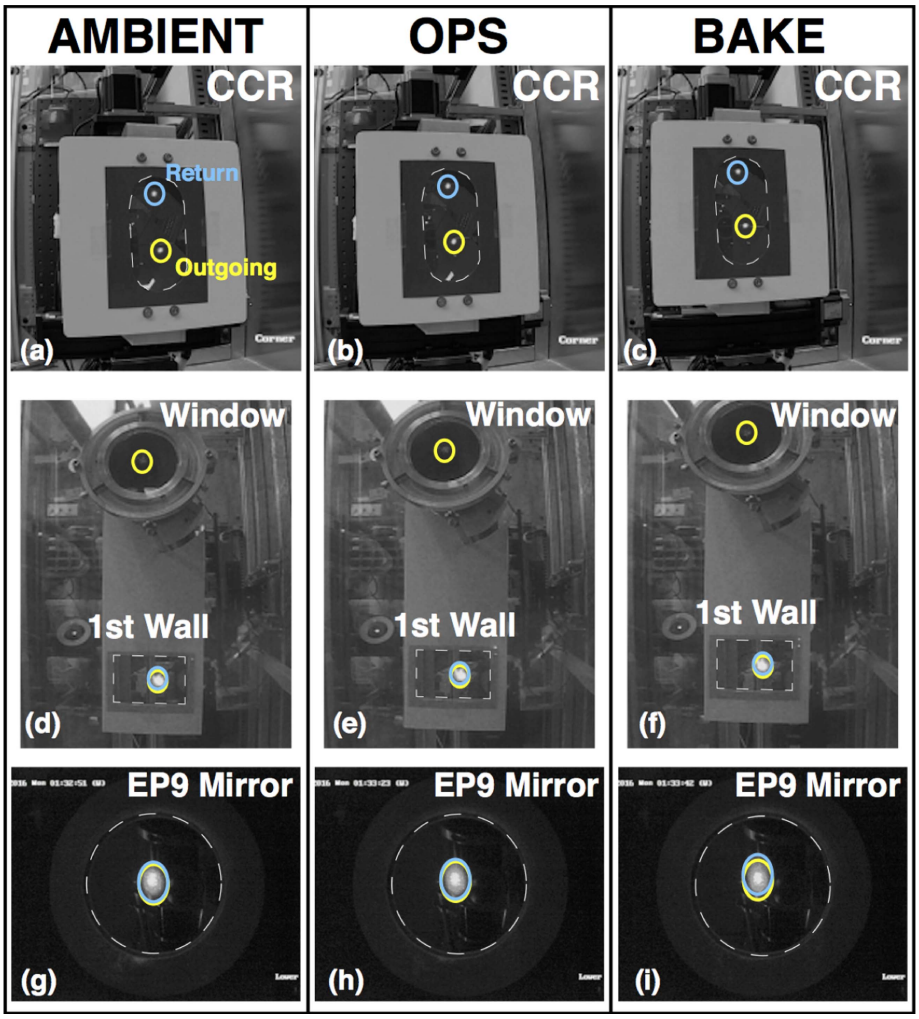

Figure 16. Camera images of beam motion on CCR, Window, 1st Wall, and EP9 mirror apertures throughout bake cycle. Yellow/blue represent outgoing/return beams.

Ambient to Bake positions and back for this scenario is available online at stacks.iop.org/PPCF/59/125005/mmedia.

3.3.2. Feedback alignment compensation for CCR distortion or 'flowering'-simulated impact of heating. To simulate the impact of CCR distortion due to heating, the tilted-facet CCR was misaligned in such a manner to simulate a flowering-like expansion of the facets. This type of distortion is the primary effect predicted by ANSYS calculations to occur due to nuclear heating during high radiation discharges. As the CCR is distorted in a flowering-like manner, it essentially removes the tilted-facet and brings it through something that is closer to a CCR with parallel incoming and outgoing beams (note, the prototype CCR is designed to have the outgoing and incoming beams overlap at the second EP9 mirror, see section 3.1.1). Eventually, the distortion becomes so large that the incoming and outgoing beams diverge rather than converge as designed. As the beams become more parallel, however, the feedback system must adjust to keep the return beam position on the optical table fixed which causes the 2nd piezo mirror to shift and the position on the CCR changes to account for this. Simultaneously, the beam separation on the last EP9 mirror increases and eventually the beams hit the edge of the EP9 aperture (100 mm diameter)—this becomes the limiting aperture. It is noted, the level of CCR distortion for this to happen is extremely large and is simply approximated by the EP9 aperture radius divided by the distance to the CCR. For this case, the intentional retro distortion is ≈50 cm/1650 cm ≈3 mRad, whereas the expected CCR thermal distortion calculated for a copper CCR due to nuclear heating is approximately 3 μm/50 mm 0.06 mRad. Camera images showing the beam positioning on the final EP9 mirror before CCR distortion and after distortion are shown in figures 17(a) and (b) respectively.

3.3.3. Failsafe alignment testing. As mentioned, a failsafe alignment system has been implemented to re-establish system

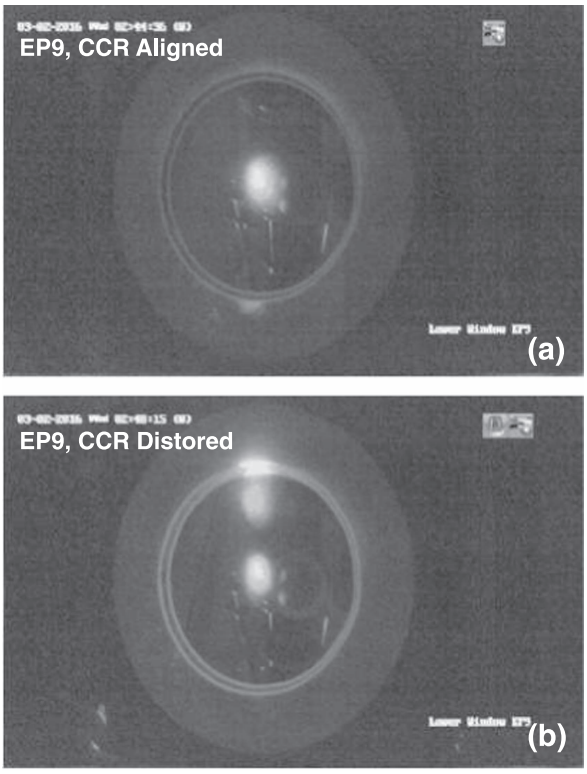

Figure 17. Camera images of beam motion on the last EP9 mirror as the CCR is intentionally distorted. (a) CCR aligned. (b) CCR distorted to failure, approximately 3 mRad.

alignment without user intervention in the event that a beam is blocked, lost, or power is somehow interrupted. Tests of these various scenarios have been carried out. Figure 18 shows the response of the feedback alignment system when both the outgoing and return beams are blocked at the EP9 window. In figure 18(a), the nominally aligned window and bioshield mirror/beam positions are shown. In panels (a)–(d), the beams are still blocked and no return beam is visible. Simultaneously, the outgoing beam can be seen executing the spiral search pattern. Since only a few frames can be shown, the actual spiral is not apparent but can be seen in a video available online. The beams are then unblocked again in figure 18(e) and the return beam becomes visible again. By the last frame shown in figure 18(f), the return beam has been found and both beams are now back at their initial positions shown in the first frame.

Similar to the beam blockage tests, the system response to loss of piezo driver voltage/power was tested. For this test, the system was brought to Ops position and the piezo driver was unplugged for each mirror then plugged back in. In each case, the system was able to recover the lost beam alignment.

4. Iter TIP prototype measurements on a full-scale beam path with feedback alignment

Building on bench tests and an initial optimization of noise floors as well as development of feedback alignment system, this section discusses extension of the TIP prototype to the full-scale beam path.

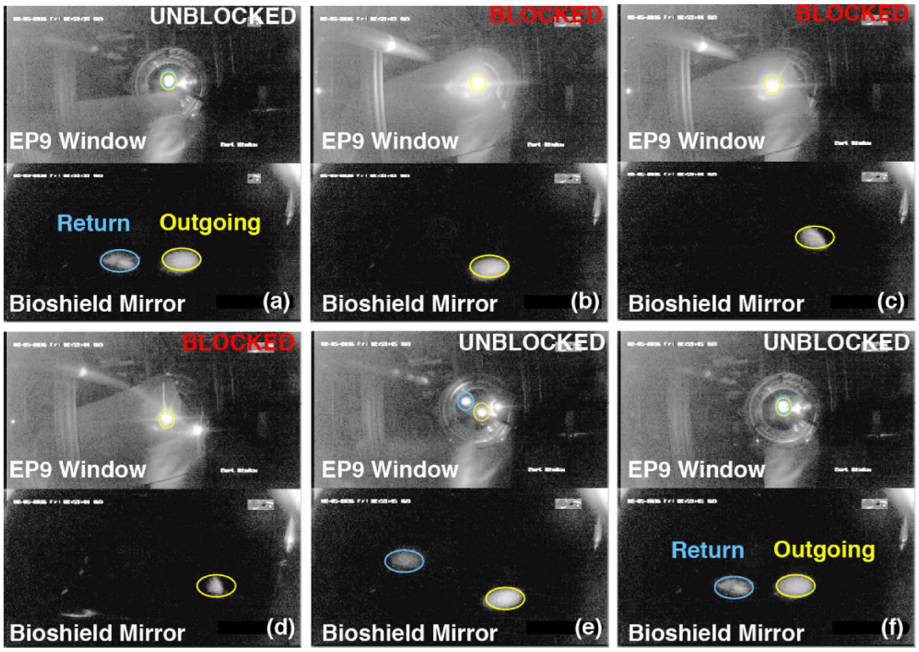

Figure 18. Feedback alignment response and recovery from blocked beam. Series of camera images showing the feedback alignment system response to blocking both outgoing (yellow) and return (blue) beams at the EP9 window. Each frame (a)–(f) shows the beam position at EP9 (top) as well as at a mirror position equivalent to the bioshield (bottom). In frames (b)–(e), the system is executing an Archimedes spiral searching for each beam.

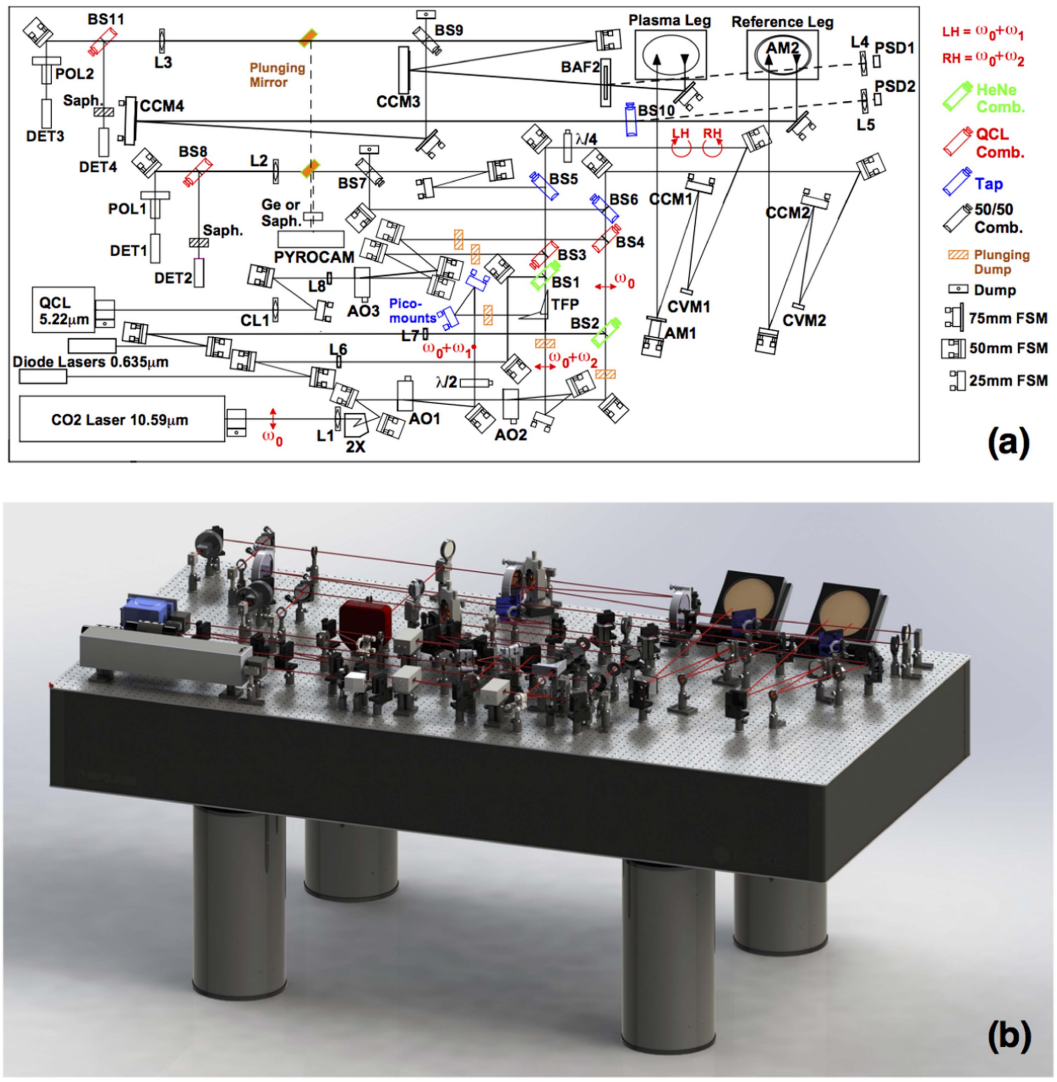

Figure 19. TIP prototype optical table layout as used for the long beam path testing. (a) Top view with each component identified. See figure 1 caption for component descriptions. New components are as follows: CVM1 and CVM2 mirrors FL = −5 cm, CCM1 and CCM2 mirrors FL = 20 cm, CCM3 and CCM4 mirrors FL = 3.18 m, AM1 = 50 mm square mirror on piezo tip/tilt platform, AM2 = 150 mm diameter mirror on piezo tip/tilt platform, PSD1 and PSD2 = visible laser position sensing detector, BaF_2 = 90 mm diameter barium fluoride window. (b) CAD model of TIP prototype optical table.

4.1. Optical table layout and measurements of beam

For extension to the 120 m beam path, considerable modification of the TIP prototype table layout was required from that used in the bench tests (figure 1). The most significant changes include the addition of optics to expand/reduce the beams sizes before/after the long beam path, a change from 632 nm HeNe lasers to 635 nm diode lasers, and the addition of feedback alignment related mirrors and sensors.

Diode lasers were used instead of the previous HeNe lasers due to the fact that the HeNe lasers were too large of a heat source in the TIP prototype enclosure and they made temperature regulation difficult. Bench tests were carried out with the HeNe lasers turned-off, however, visible lasers are needed in the long beam path implementation for feedback alignment. Additionally, the diode lasers used are 8 mW each so more signal is available for feedback alignment position sensing. Beam expansion is required to maintain a relatively collimated beam and tractable beam sizes at the end of the 120 m beam path. This is accomplished using a convex (CVM) and concave mirror (CCM) with focal lengths of −50 mm and 200 mm respectively (CVM1 and CCM1) to form a 4× expander. After returning to the optical table, the beams are reduced by a set of 3.18 m focal length concave mirrors (CCM3 and CCM4).

Also included on the optical table are active mirrors for both the plasma and reference legs labeled AM1 and AM2 respectively. As mentioned, the plasma leg uses two active mirrors, one of which is located near the window and AM1

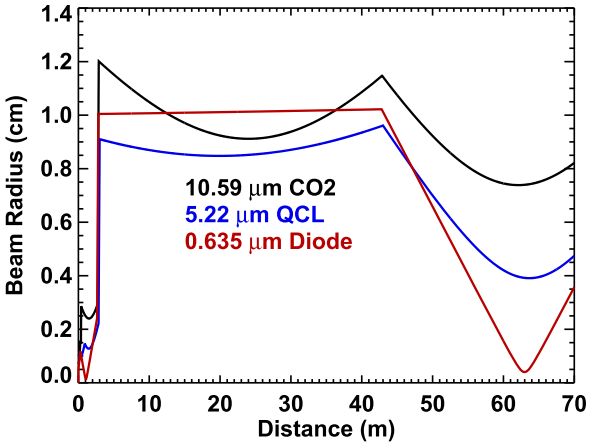

Figure 20. Gaussian beam calculations for all lasers along the full beam path.

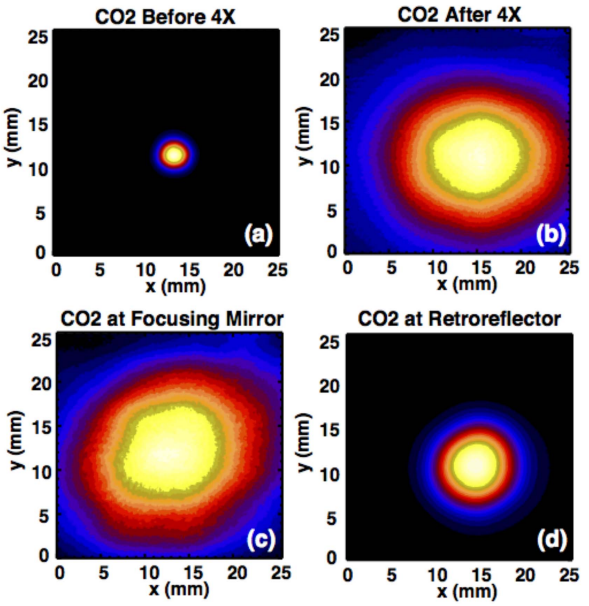

Figure 21. Measured CO_2 laser beam profiles at four locations along long beam path.

which is located on the table. The plasma leg active mirror AM1 is a 50 mm square mirror on a 25 mm piezo tip/tilt mount. The reference leg uses a single active mirror feedback system with a larger 50 mm tip/tilt platform and a 150 mm diameter mirror. Both feedback systems are open loop and based primarily on visible laser position sensors labeled PSD1 and PSD2 in figure 19. Beam sampling for the position sensors on the optical table is accomplished by a 91 mm diameter BaF_2 window on the plasma leg (labeled BaF_2) and a ZnSe splitter labeled BS10 on the reference leg.

The expander and focusing mirror placement has been optimized to minimize the overall beam size along the full beam path as well as on the retroreflector. Results of Gaussian beam calculations used to guide the layout are shown in figure 20. After installation, beam profiler measurements of the CO_2 and QCL beam profiles were made at several locations along the extended beam path. An example of these measurements is shown in figure 21. A comparison of the measured beam waist radii with that predicted from the Gaussian beam calculations at various positions along the beam path is given in table 2, where the measured radii are obtained from Gaussian fits to the beam profiler measured beam spots.

Reasonable agreement with the predicted beam sizes is found, however, the CO_2 beam is slightly larger than expected when it reaches the focusing mirror at EP9. In turn, this causes the beam to be slightly smaller at the CCR.

4.1.1. Matching plasma and reference leg path lengths on long beam path. As discussed in section 2.2.1, matching plasma and reference leg path lengths is an important issue for low-noise interferometric measurements. This is a non-trivial task on a 120 m beam path with many components spanning three rooms. Fortunately, the QCL can be operated in pulsed mode with pulse durations as low as 40 ns. This allows a sensitive time-of-flight measurement to be made which identically traces the full optical train and provides a measure of all relevant beam paths. In figure 22, measurements are presented showing a pulse arriving at the optical LO detector then arriving approximately 393 ns later at the plasma and reference leg detectors. Note, to make this measurement the plasma and reference leg measurement are made one at a time since they share a common detector. The measurements show an initial path difference of 2.6 ns (≈80 cm) obvious in difference between received reference and plasma pulses. After identification of this difference, the reference leg CCR was moved by the appropriate amount.

Alternatively, building on the results presented in figure 6, the increase in interferometric phase noise with path length mismatch can actually be used to fine tune the path length matching. This is similar to length measurement using Optical Coherence Tomography. Here, the QCL phase noise is measured as the plasma leg CCR is displaced in small 2.5 mm steps. The results have a minimum in integrated phase noise both from the QCL alone as well as the vibration compensated phase at the exact position at which the reference ad plasma legs are matched.

4.2. Full-scale beam path TIP prototype test results

Part of the evaluation of the feedback alignment system and determining an optimum strategy depends on not only how well the system can keep the beam on the long optical train, but how it impacts the interferometer and polarimeter measurements. The following sections directly compare vibration compensated interferometer and polarimeter measurements with and without feedback alignment as the system is subjected to various sources of motion.

To simulate an actual experiment, initial alignment is carried out at the Ambient position, measurements are made, then the system is moved through Bake then to the Ops

Table 2. Comparison between measured and predicted beam waist radii at various positions along the beam path.

Location	Calculated radius CO_2 beam (mm)	Measured radius CO_2 beam (mm)	Calculated radius QCL beam (mm)	Measured radius QCL beam (mm)
Before expander	2.6	2.2	1.7	1.8
After expander	11.9	11.7	9.1	9.0
Focusing mirror	11.6	15.2	9.5	8.0
At CCR	7.4	6.0	3.8	3.6

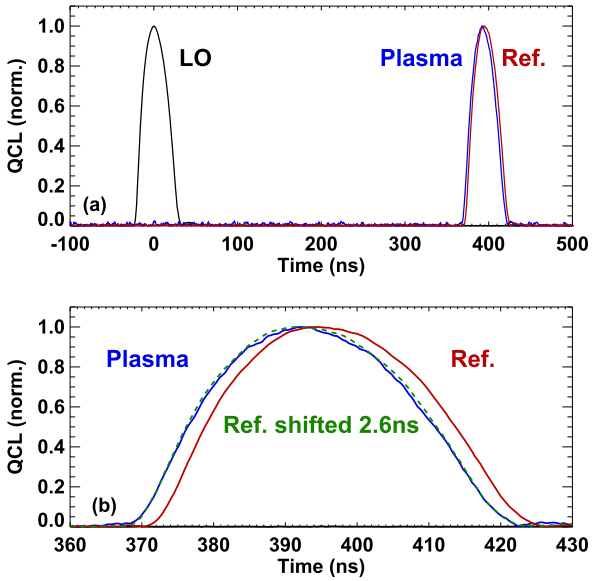

Figure 22. (a) QCL pulses used to measure reference and plasma leg path lengths. (b) Zoomed in region of plasma and reference leg pulses showing relative arrival times. Dashed curve is the reference pulse shifted by 2.6 ns.

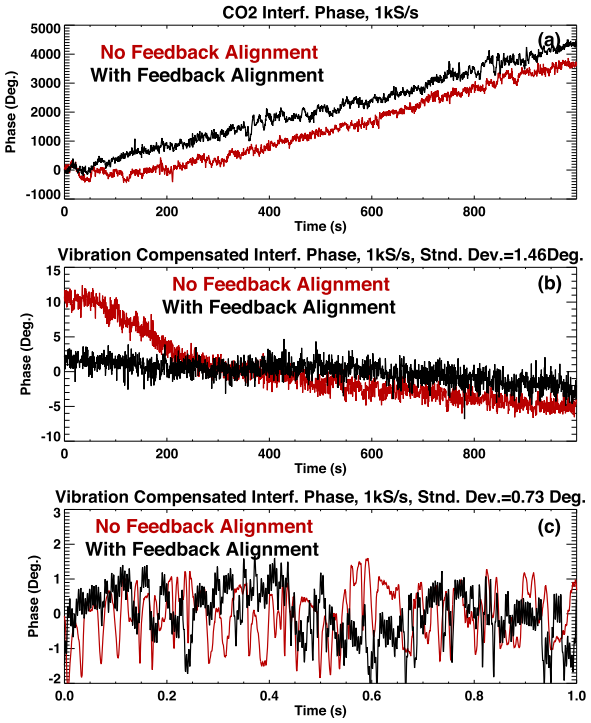

Figure 23. Interferometer phase data with (black) and without (red) feedback alignment at Ops position. (a) Uncompensated CO_2 interferometer phase. (b) Vibration compensated phase. (c) Vibration compensated phase over 1 s interval.

position where the bulk of measurements and alignment sensitivity tests are carried out. Initial measurements after moving to the Ops position showed the system is able to maintain feedback alignment and both interferometer interference and polarimeter signals. Interferometer measurements over a 1000 s interval at the Ops position with and without feedback alignment are shown in figure 23 where the vibration compensated interferometer noise is found to be $\delta\phi_{\rm int} = 0.8^\circ$ with feedback alignment and significantly larger without it (figure 23(b)). Measurements over a shorter 1 s interval show the vibration compensated noise floors are comparable with and without feedback alignment (figure 23(c)).

Polarimeter measurements over the same 1000 s interval at the Ops position are shown with and without feedback alignment in figure 24. Similar to the interferometer measurements, polarimeter noise is observed to increase significantly without feedback alignment. The polarimeter noise floor is $\delta\phi_{\rm pol} = 0.06^\circ$ over the 1000 s interval (figure 24(b)) and $\delta\phi_{\rm pol} = 0.05^\circ$ over a shorter 1 s interval (figure 24(c)). Without feedback alignment a slow timescale polarimeter drift of $\approx 0.3^\circ$ occurs with occasional intermediate excursions of up to $\approx 0.4^\circ$. These results are extremely encouraging and show the system is already able to meet ITER's measurement requirements of $\delta\phi_{\rm pol} = 0.1^\circ$ and $\delta\phi_{\rm int} = 10^\circ$ with measured phase resolution of $\delta\phi_{\rm pol} = 0.06^\circ$ and $\delta\phi_{\rm int} = 1.5^\circ$ over a full 1000 s shot duration.

As mentioned in the bench test section, oscillation of the plasma leg CCR parallel to the beam path is an excellent way to check the functionality of the vibration compensated interferometer and polarimeter system. Interferometer measurements with the plasma leg retroreflector oscillating $\delta Y = \pm 5$ mm parallel to the beam path (± 1 cm path length changes) are shown in figure 25. The top panel shows shows the corresponding QCL, CO_2 laser, and vibration compensated phases where, even in the presence of 10^5 degree phase changes, the vibration compensated phase noise is $\delta\phi_{\rm int} = 0.95^\circ$ over the 80 s interval (see figure 25(b)).

Figure 25 shows motion parallel to the beam path and provides a test of the TIP prototype vibration compensation ability. Intentionally introducing motion perpendicular to the

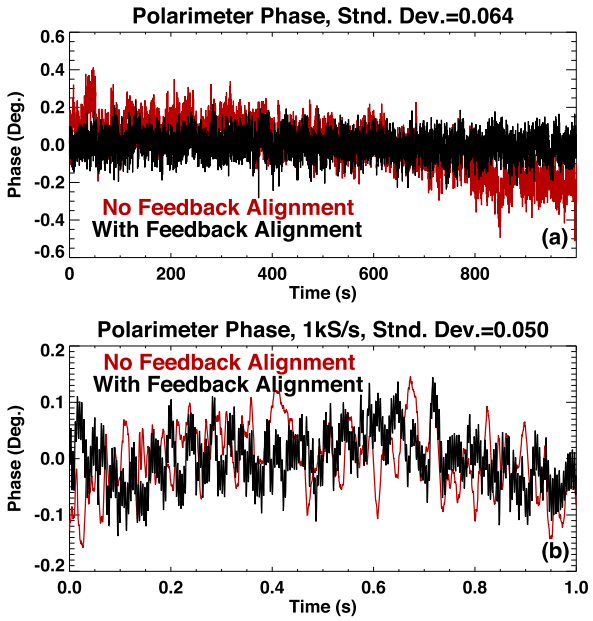

Figure 24. Polarimeter noise floor with (black) and without (red) feedback alignment at Ops position. Polarimeter phase over 1 s interval.

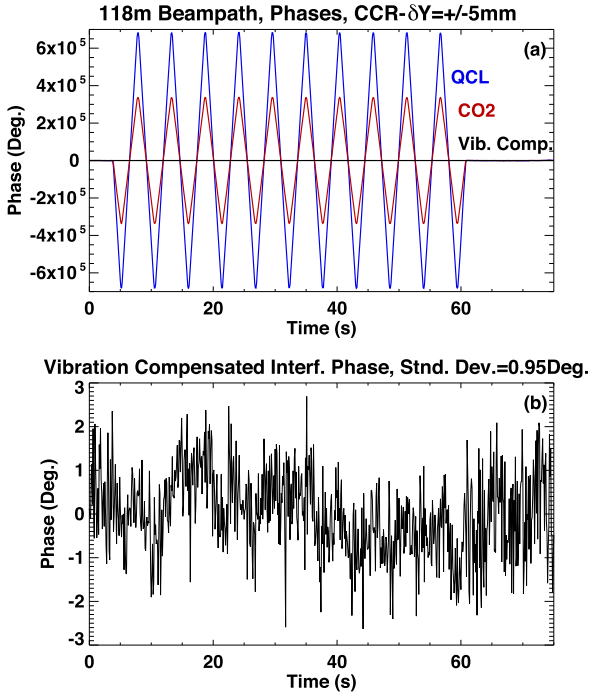

Figure 25. CO_2, QCL and vibration compensated phases during ± 5 mm CCR motion at Ops position. (a) QCL, CO_2 and vibration compensated phase. (b) Vibration compensated phase only.

beam path however tests both the feedback alignment system and the TIP's sensitivity to motion. Figure 26 shows the vibration compensated interferometer response to ± 5 mm jogs (the same sequence as in figure 25) on each of the three

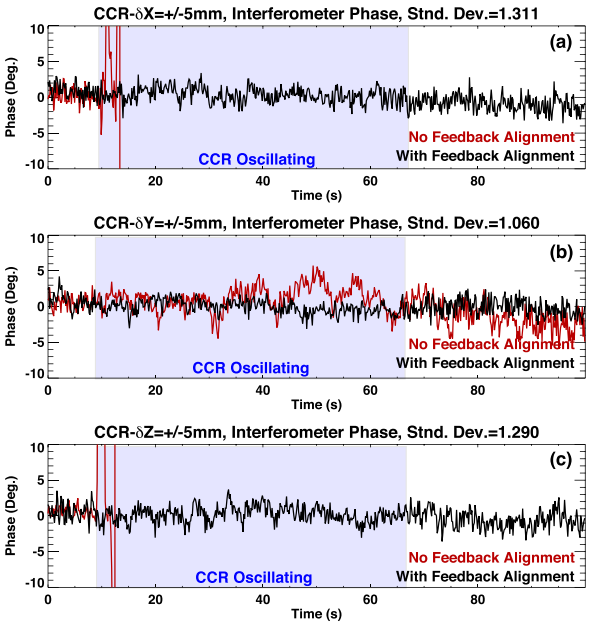

Figure 26. CCR motion impact on vibration compensated interferometer noise at Ops position. (a)–(c) are for horizontal, parallel, and vertical motion relative to the beam path respectively.

stage axes. Figures 26(a)–(c) are for horizontal, parallel, and vertical motion relative to the beam path respectively. As can be seen, for either of the cases with motion perpendicular to the beam path figures 26(a) and (c), the interferometer immediately becomes misaligned and the vibration compensated phase fringe skips occur. In all cases with feedback alignment enabled, the vibration compensated interferometer signal is relatively unaffected and the noise remains at approximately $\delta\phi_{\mathrm{int}} = 1.3^{\circ}$ or lower.

Polarimeter data during the same CCR oscillations are shown in figure 27 where a similar immunity to the motion is found when feedback alignment is enabled. With feedback alignment, polarimeter noise remains at $\delta\phi_{\mathrm{pol}} = 0.06^{\circ}$ or lower and without feedback alignment, it can reach several degrees during the CCR oscillations, particularly those perpendicular to the beam path. Further, some of the polarimeter phase shift being included in the noise estimate with feedback alignment enabled is actually expected and due to the 4 MHz frequency difference in the R and L waves, similar to that shown explicitly in figure 8.

In addition to CCR motion, the beam path simulator is able to oscillate all of the EP9 optics vertically and/or parallel to the incoming beams. This includes moving the window (with feedback alignment sensor, EP9 mirrors, and first wall apertures). Tests like those shown above for CCR motion except with EP9 moving yield similar conclusions. With feedback alignment enabled, vibration compensated interferometer and polarimeter data noise floors are low and for transverse motion, feedback alignment is essential. Moreover, since the beams traverse EP9 twice, $\delta Y = \pm 5$ mm motion corresponds to ± 2 cm of path length change. The fact that the TIP system is able to follow such a large phase shift

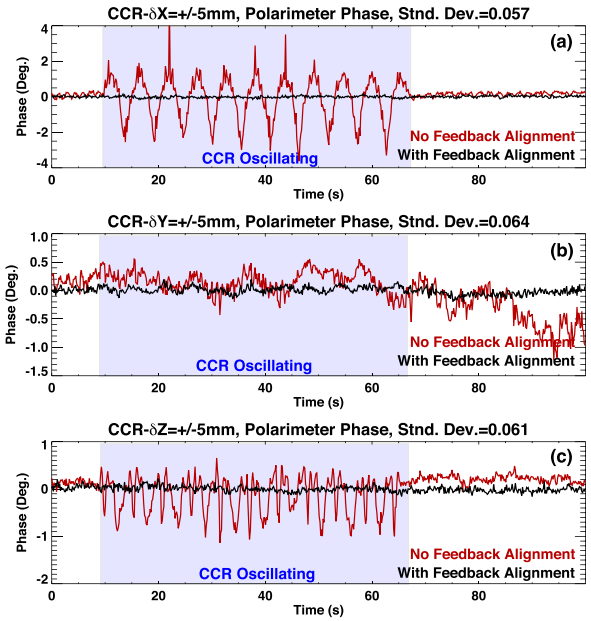

Figure 27. CCR motion impact on polarimeter noise at Ops position (a)–(c) are for horizontal, parallel, and vertical motion relative to the beam path respectively.

($\pm 1.4 \times 10^6$ degrees for the QCL) and still maintain $\delta\phi_{\text{int}} = 1.3^\circ$ phase noise with no drift, is an excellent demonstration of the large dynamic range and accuracy of the system. As with the CCR motion, perpendicular oscillations of EP9 result in an immediate loss of vibration compensated interferometer phase while with feedback alignment the interferometer and polarimeter have no problem tracking the phase.

4.2.1. R and L wave misalignment and impact on noise floor. Both the interferometer and polarimeter are obviously sensitive to alignment. Feedback alignment is used to keep the system aligned after the two colors and R and L wave beams are prepared. For effective vibration compensation, the two colors must be collinear and similarly, so must the R and L waves. Additionally, the polarimeter must have excellent co-alignment of the R and L waves to avoid contamination from density gradient induced interferometric phase contamination. This co-alignment is accomplished using the beam profiler and remote mount approach presented in section 2.1.3. Figure 28 addresses the vibration/motion induced phase noise in the vibration compensated interferometer and polarimeter as the beams are intentionally misaligned.

In this test, the far-field Picomotor mount in figure 19 is intentionally steered from perfect alignment such that the vertically polarized 10.59 μm beam is progressively misaligned in the vertical and horizontal directions. The beam misalignment is documented using the far-field plunging mirror and beam profiling camera. The spatial profiles as the beam is moved two remote mount jogs ($\approx 1/5$ beam radius after returning to table) at a time in either direction are shown

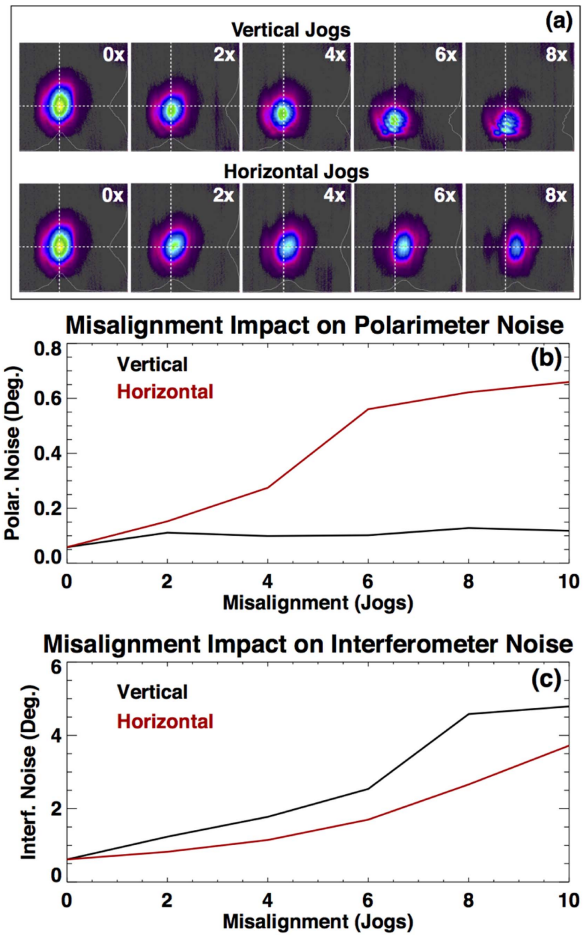

Figure 28. (a) Far-field CO_2 beam profiles during intentional misalignment of 40 MHz plasma leg and impact on (b) polarimeter and (c) vibration compensated interferometer noise. Dashed lines in (a) indicate nominally aligned position.

in figure 28(a). At each position, data are acquired over a 100 s during which the CCR stage executing $\delta Z = \pm 2$ mm oscillations for 15 s of the window. The results show first of all that there is a significant increase in noise for both the interferometer and polarimeter as the beams are misaligned, and second that this noise is not increased symmetrically for vertical and horizontal misalignment. It is noted that the results of these tests are the same whether or not the noise is calculated over the interval during which the CCR oscillations are occurring.

Polarimeter noise increases drastically with misalignment. In fact for a misalignment of $\approx 1/4$ beam radius, the noise increases above the $\delta\phi_{\text{pol}} < 0.1^\circ$ target value. For the polarimeter, the increase in noise is also very different for the vertical and horizontal directions. It is speculated that this asymmetry could be due to the clear difference in beam profiles for the different steering directions (figure 28(a)).

4.2.2. Atmospheric impact on TIP prototype. Beam power is significantly reduced after transiting the long beam path on

Table 3. Measured and predicted transmission based on theoretical reflectivities after transmission along the extended beam path.

Wavelength (μm)	Launch (mW)	Return (mW)	Transmission (%)	Expected trans. (%)
10.591—plasma	630	120	20	30 ± 6
10.591—ref.	380	62	16	32 ± 4
5.22—plasma	50	<2	<4	30 ± 5
5.22—ref.	31	<2	<6	40 ± 5

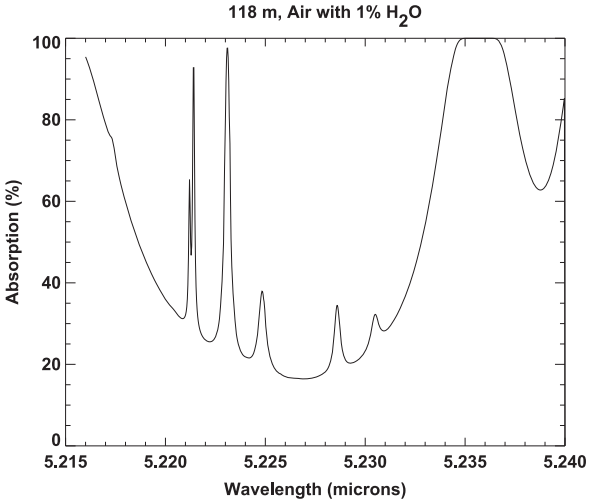

Figure 29. Mid-IR absorbtion spectrum for air with 1% H_2O and 118 m beam path.

both the plasma and reference legs. Due to the large number of reflections, considerable attenuation is expected. A comparison of the measured and expected transmissions over the long beam path measured just before leaving and after returning to the TIP optical table are shown in table 3.

The CO_2 laser 10.591 μm attenuation is larger than expected but it is likely some disagreement should be anticipated due to the fact that the expected transmission is based on theoretical estimates of the S and P reflectivities of the various components. The 5.22 μm QCL attenuation, however, is very large and in fact the numbers presented are upper estimates based on the fact that the power meter used was inadequate for measurements below 2 mW. This large attenuation has been traced to a large attenuation on water vapor in the atmosphere and is discussed below. Interestingly, even with such low return powers, excellent interferometer phase resolution is obtainable.

The unexpectedly large attenuation of 5.22 μm QCL power was measured again at several positions and was found to be attenuated roughly equally on both the reference and plasma legs. Additionally, the fractional power attenuation is linear with distance (40 mW launch, 8 mW at CCR, 1−2 mW after return to table). All of the data indicate this excess absorption is not due to any particular optic but rather absorption is occurring in the atmosphere, the source of which was traced to H_2O in atmosphere as described below.

The nominal center wavelength of the QCL used here is 5.2262 μm with ≈16% expected absorption on H_2O along 120 m beam path. After closer analysis, however, the laser was

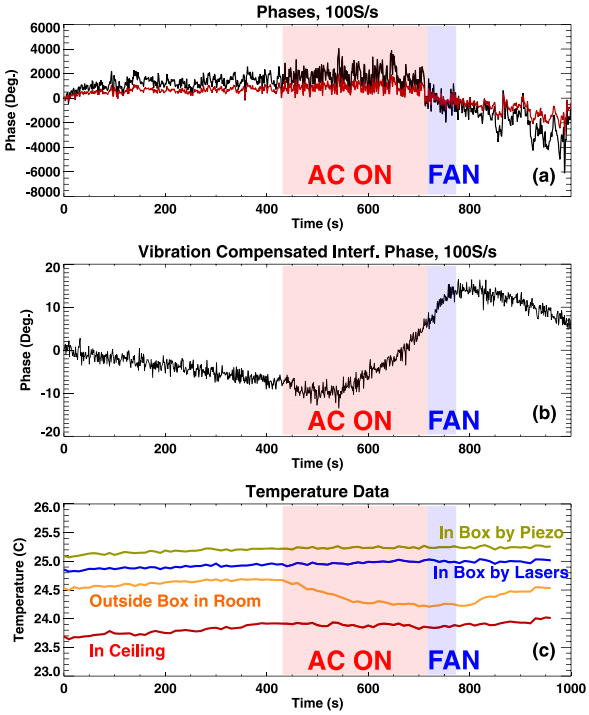

Figure 30. Drift induced in vibration compensated interferometer phase due to air conditioning and operation at 5.2169 μm. Air conditioning is on during period $t \approx$ 430–720 s. (a) CO_2 phase (red) and QCL phase (black). (b) Vibration compensated phase. (c) Temperature measurements at different locations.

found to be operating in the range 5.216–5.219 μm (depending on the setpoint), where absorption increases rapidly (see figure 29). The QCL wavelength can be tuned 2 nm through the controller (varies internal head temperature ±5 °C about nominal 20 °C temperature). To verify the absorption was really on H_2O, the QCL wavelength was varied from 5.2177 to 5.2183 μm. This small variation resulted in reference leg return power increasing by 35% and plasma leg return power increasing by 48%. Assuming 1% H_2O in atmosphere, HITRAN [28] calculations predict a 36% increase—consistent with measurements. One unexpected, but potentially positive, result is that this scanning ability allows the QCL to measure line-integrated humidity levels.

Such a large absorption on H_2O can imply significant refractive index changes with humidity, a factor that has practical implications for the current TIP prototype and can cause significant drifts in vibration compensated interferometer phase when the QCL is operating in the 5.216–5.217 μm

range (see figure 29) and similarly for 10.59 μm dispersion interferometer (DI) [25, 29, 30] systems. Increased lab temperatures, such as were experienced during a portion of these tests, require air conditioning to maintain the <24.7 °C setpoint. Approximately 50 m of plasma leg beam path are housed in the AC controlled room and are exposed to rapid changes in humidity when the TIP laboratory air conditioner comes on, the effect of which on vibration compensated interferometer measurements is shown in figure 30. Both nitrogen and clean dry air purges were also tested on the TIP prototype long beam path. Consistent with above findings, QCL return power increased significantly. Vibration compensated interferometer measurements however showed large dispersion and optical path length changes with no steady state reached after one hour of purging. This is to be expected since the current beam lines are not sealed tightly and the entire bottle of each gas was emptied in under 2 h. If a purge is to be pursued further (which is likely not required both due to the fact that the QCL will be changed to its original specification wavelength of 5.2262 μm and that the actual ITER TIP will use 4.6 μm), it would require specifically designing the beam path for this with appropriate seals. Alternatively, a low level vacuum could also be considered. It is pointed out that this interaction with H_2O vapor will impact long path length 10.59 μm DI systems with doubled wavelength of 5.2955 μm. For those systems, the expected absorption on 120 m path is ≈80%.

Fortunately, the 5.22 μm QCL being used for the prototype was only chosen to be compatible with 5.42 μm CO laser optics previously procured by GA and TIP project. It is envisioned that the actual ITER TIP will use a 4.6 μm QCL which has essentially no nearby absorption lines and 10× higher operating power while also increasing the effective density resolution by ≈10% due to the shorter wavelength.

5. Summary, conclusions and future work

Significant progress has been made toward a viable design for the ITER toroidal interferometer/polarimeter including the construction of a full-scale prototype complete with feedback alignment. In the process of this R&D effort, several new TIP elements have been tested, issues identified and solutions developed—essentially all of which have been incorporated in some way into the current ITER TIP design discussed briefly below. A list of several of the key accomplishments and technical results is given below:

- A 120 m path length TIP prototype based on a two-color interferometry measurement at 10.59 and 5.22 μm using a CO_2 and QCL respectively combined with a polarimetry measurement at 10.59 μm beams has been constructed. The prototype incorporates translation stages to simulate ITER motion through a bake cycle as well as other sources of motion or misalignment (sections 3 and 4).
- The full 120 m beam path TIP prototype is able to meet ITER's density measurement requirements over 1000 s shot durations with demonstrated phase resolution of 0.06° and 1.5° for the polarimeter and vibration compensated interferometer respectively (figures 23 and 24). The ITER specified values implied from density measurement requirements are 0.1° and 10°.
- Feedback alignment is found to be essential to meeting ITER's measurement requirements and, with feedback alignment enabled, both the interferometer and polarimeter are able to withstand slow timescale transverse (≈±0.5 cm) and several centimeter parallel displacements of in-vessel optics while still maintaining performance (figures 26 and 27).
- TIP vibration compensated interferometer measurements of a plasma have been made in a pulsed RF device. These data represent the first measurement of a plasma by a combined CO_2/QCL two-color interferometer and polarimeter and show a line-integrated density resolution of $\delta nL = 3.5 \times 10^{17}$ m^{-2} (figure 12).
- An important design feature of the TIP prototype which enables precise, stable, remote, and easily automated co-alignment of all necessary beams is the use of a beam profiling camera combined with Picomotor™ remote actuated mounts (section 2.1.3).
- A QCL offers a reliable turn-key solution for the shorter wavelength vibration compensation laser, originally specified at the TIP conceptual design review [4] to be 5.42 μm CO laser (section 2.1.2).
- Significant attenuation of the 5.22 μm beam by water vapor on the long beam path has been observed and can lead to phase drifts. To avoid this in future implementations, a QCL operating at 4.6 μm is suggested for vibration compensation. These results also indicate that DIs operating at 10.59 and 5.3 μm will experience significant absorption of the shorter wavelength beam and experience possibly larger drifts (section 4.2.2).
- Precise temperature control of the TIP optical table is required to maintain alignment of the various TIP beams, an essential element for low-noise interferometry and polarimetry measurements (section 2.1.1).
- A novel, intentionally misaligned retroreflector designed to have a crossover point near the first wall, with the goal of minimizing penetration sizes, has been implemented and appears to work well (section 3.1.1).
- To lower interferometer noise, a reference leg with path length matched to that of the plasma leg will be required. This path length matching can be accomplished precisely using the QCL in either pulsed mode for a time-of-flight measurement or by minimizing large bandwidth phase noise fluctuations (sections 2.2.1 and 4.1.1).

Future work will include moving the TIP prototype from the extended beam path lab to the DIII-D tokamak where measurements of plasmas will be made with both the interferometer and polarimeter. Simultaneously, engineering design and simulation work on the actual ITER TIP implementation is ongoing in preparation for a preliminary design review.

Acknowledgments

This work is supported by US DOE Contract numbers DE-AC-02-09CH11466. PPPL Prime Contract Number is DE-AC-02-09CH11466. All US activities are managed by the US ITER Project Office, hosted by Oak Ridge National Laboratory with partner labs Princeton Plasma Physics Laboratory and Savannah River National Laboratory. The Project is being accomplished through a collaboration of DOE Laboratories, universities and industry. The views and opinions expressed herein do not necessarily reflect those of ITER Organization.

References

[1] Donne A J H *et al* and the ITPA Topical Group on Diagnostics 2007 *Nucl. Fusion* **47** S337
[2] Carlstrom T N *et al* 1998 Baseline design of a multi-channel interferometer and polarimeter system for density measurements on ITER *Diagnostics for Experimental Thermonuclear Fusion Reactors 2* ed P E Stott *et al* (New York: Plenum)
[3] Kondoh T *et al* 2004 *Rev. Sci. Instrum.* **75** 3420
[4] Van Zeeland M A *et al* 2013 *Rev. Sci. Instrum.* **84** 043501
[5] Baker D R and Lee S T 1978 *Rev. Sci. Instrum.* **49** 919
[6] Lehecka T, Peebles W A, Luhmann C and Carlstrom T N 1988 *Rev. Sci. Instrum.* **8** 1580
[7] Carlstrom T N, Ahlgren D R and Crosbie J 1988 *Rev. Sci. Instrum.* **7** 1063
[8] Kawano Y *et al* 1996 *Rev. Sci. Instrum.* **67** 1520
[9] Innocente P *et al* 1997 *Rev. Sci. Instrum.* **68** 694
[10] Dodel G and Kunz W 1978 *Infrared Phys.* **18** 773
[11] Kunz W and Equipe TFR 1978 *Nucl. Fusion* **18** 1729
[12] Akiyama T *et al* 2003 *Rev. Sci. Instrum.* **74** 2695
[13] Van Zeeland M A *et al* 2008 *Rev. Sci. Instrum.* **79** 10E719
[14] Ding W X, Brower D L, Bergerson W F and Lin L 2010 *Rev. Sci. Instrum.* **81** 10D508
[15] Mirnov V V *et al* 2007 *Phys. Plasmas* **14** 102105
[16] Mirnov V V *et al* 2013 *Nucl. Fusion* **53** 113005
[17] ITER Document IS-47-55.C5-018
[18] Rommers J H and Howard J 1996 *Plasma Phys. Controlled Fusion* **38** 1805
[19] Rommers J H, Donne A J H, Karelse F A and Howard J 1997 *Rev. Sci. Instrum.* **68** 1217
[20] Brower D L *et al* 2001 *Rev. Sci. Instrum.* **72** 1077
[21] Brower D L *et al* 2003 *Rev. Sci. Instrum.* **74** 1535
[22] Ding W X *et al* 2004 *Rev. Sci. Instrum.* **74** 3387
[23] Akiyama T *et al* 2001 *Rev. Sci. Instrum.* **72** 1073
[24] Van Zeeland M A, Boivin R L, Carlstrom T N, Deterly T and Finkenthal D K 2006 *Rev. Sci. Instrum.* **77** 10F325–1
[25] Bamford D J *et al* 2013 *Rev. Sci. Instrum.* **84** 093502
[26] ITER_D_3T85AQ v 2.0
[27] Lilje L *et al* 2002 *Proc. EPAC (Paris, France)*
[28] http://hitran.org
[29] Bagryansky P A *et al* 2006 *Rev. Sci. Instrum.* **77** 053501
[30] Akiyama T, Yasuhara R, Kawahata K, Okajima S and Nakayama K 2014 *Rev. Sci. Instrum.* **85** 11D301